Non-Covalent Assembly of Proton Donors and *p*-Benzoquinone Anions for Co-Electrocatalytic Reduction of Dioxygen

Supporting Information

Shelby L. Hooe, Emma N. Cook, Amelia G. Reid, Charles W. Machan*

* - machan@virginia.edu; ORCID 0000-0002-5182-1138

- S.L.H. ORCID 0000-0002-6991-2273; E.N.C. ORCID 0000-0002-0568-3600; A.G.R ORCID 0000-0002-2868-4091

Department of Chemistry, University of Virginia, PO Box 400319, Charlottesville, VA 22904-4319

Table of Contents:

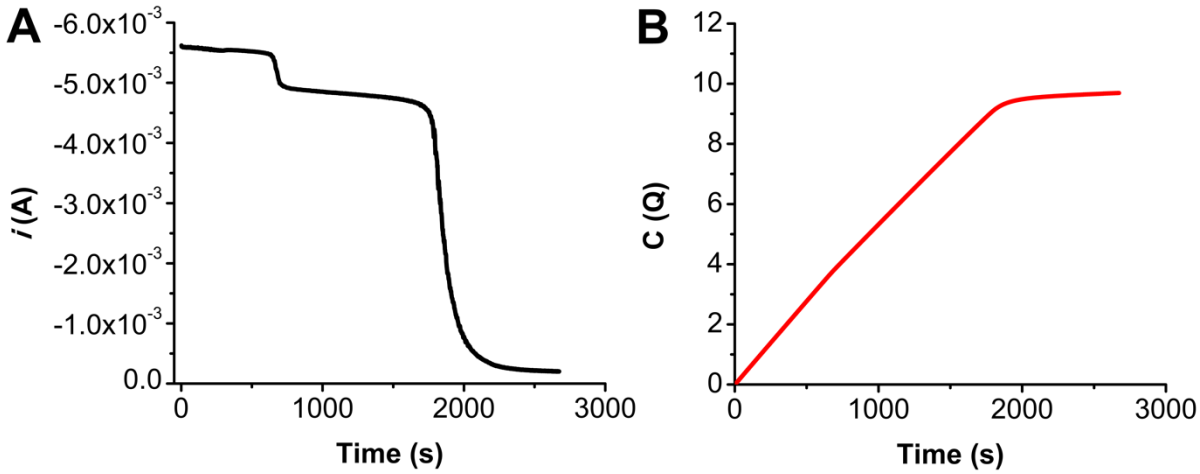

Figure S1. Coulometry experiment with 2.5 mM BQ in an MeCN solution under N_2 saturation conditions. The analyte solution volume was 25 mL, containing a total of 6.25 x 10^{-5} moles of BQ and passing a total of 9.7 C of charge. Conditions: 0.1 M $TBAPF_6$/MeCN; Carbon cloth (Plain Carbon Cloth 1071 from FuelCellStore) working and counter electrodes; Ag/AgCl pseudoreference electrode. Applied potential of –2.1 V vs. Fc^+/Fc.

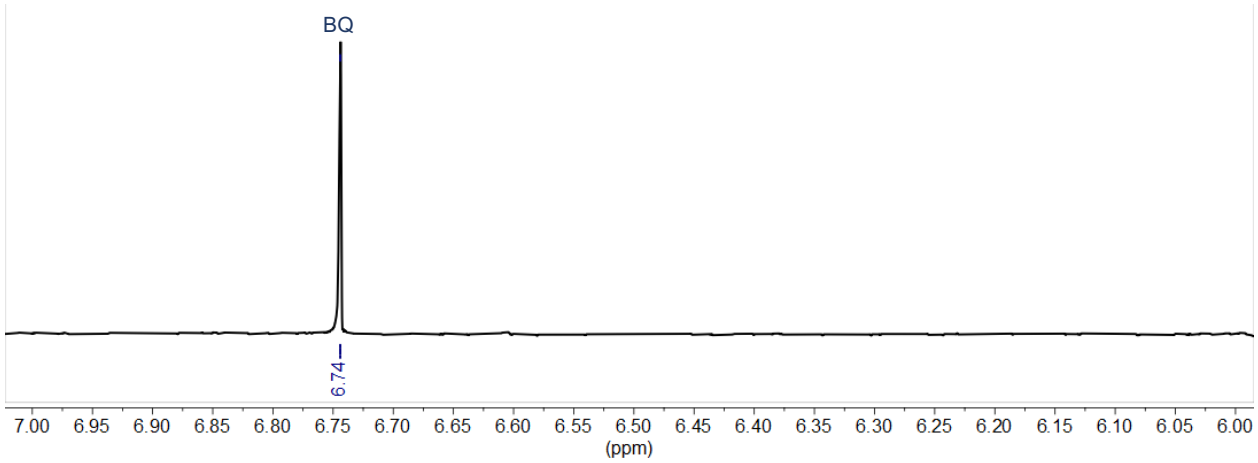

Figure S2. ^1H NMR of an authentic BQ sample taken prior to coulometry experiment in **Figure S1** under an atmosphere of N_2. The ^1H NMR sample was prepared from a 3:1 mixture of coulometry experiment solution and CD_3CN, respectively. The aromatic peak at 6.74 ppm corresponds to BQ under aprotic and inert conditions.

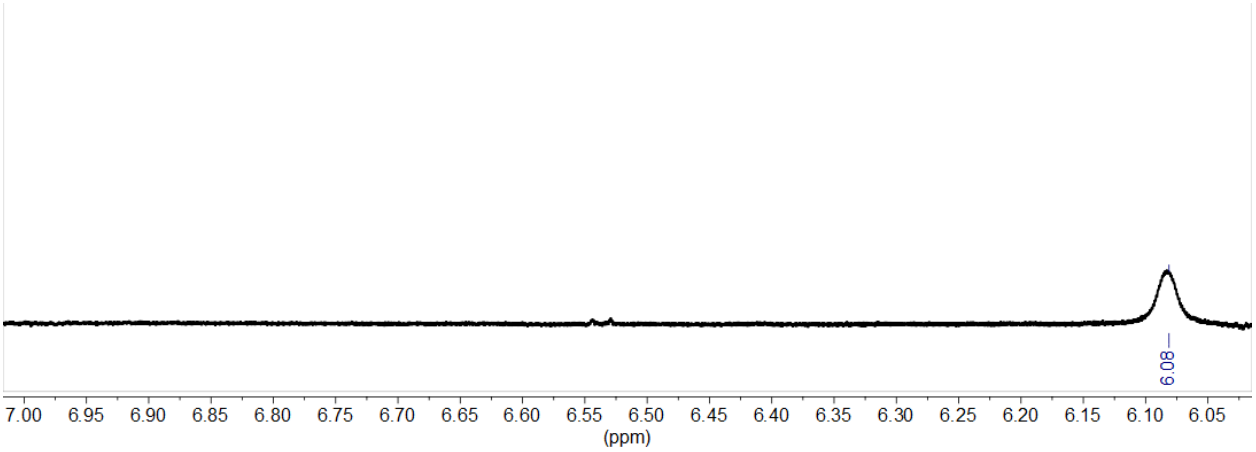

Figure S3. ^{1}H NMR spectrum of an authentic $[BQ]^{2-}$ sample taken after coulometry experiment in **Figure S1** under an atmosphere of N_2. ^{1}H NMR solution was prepared from a 3:1 mixture of coulometry experiment solution and CD_3CN, respectively. The peak at 6.08 ppm corresponds to the two-electron reduced product of BQ under aprotic and inert conditions. Additionally, the absence of a peak at 6.74 ppm corresponding to BQ indicates complete substrate consumption from the coulometry experiment in **Figure S1**.

Table S1. Data from variable TFEOH concentration CV data with 0.5 mM BQ (**Figure 2A**).

[TFEOH(M)]	$E_{1/2}$ (V vs. Fc^+/Fc)	ΔE_p (V)
0.0000	-0.891	0.0736
0.00130	-0.889	0.0728
0.00260	-0.887	0.0738
0.00400	-0.886	0.0756
0.00530	-0.885	0.0718
0.00660	-0.884	0.0738
0.0264	-0.870	0.0776
0.0528	-0.850	0.0838
0.132	-0.801	0.0985
0.198	-0.769	0.117
0.264	-0.742	0.151
1.37	n/a	n/a

*Potential values in table correspond to data for the most positive BQ reduction potential, which has been characterize as a two-electron redox process when TFEOH is present as illustrated in coulometry experiments.

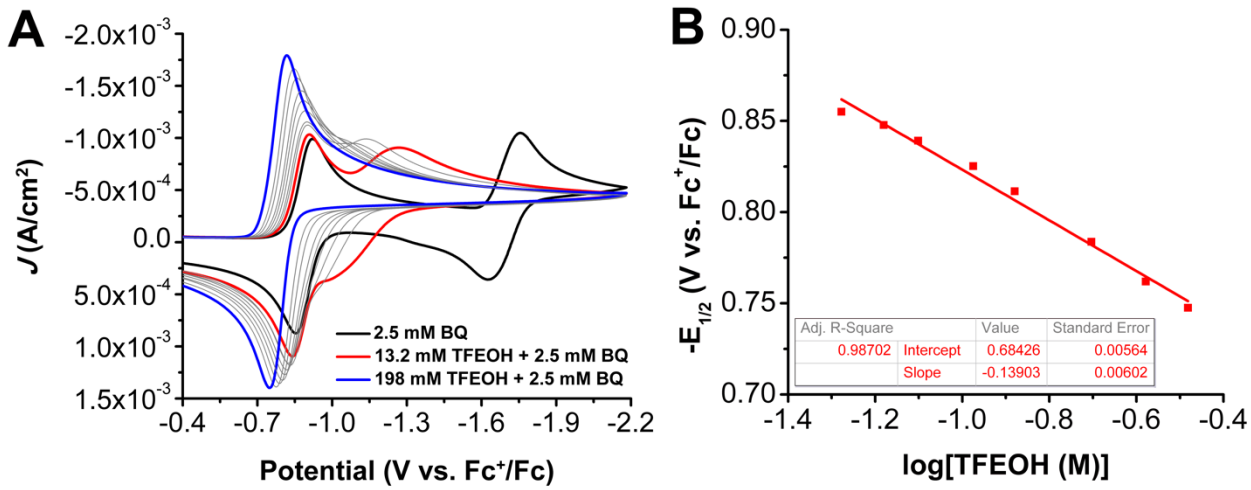

Figure S4. (**A**) CVs of TFEOH titration with 2.5 mM BQ obtained under Ar saturation conditions. (**B**) Linear fit of $-E_{1/2}$ versus log[TFEOH (M)] for the two-electron BQ reduction feature observed between –0.75 and –0.86 V vs. Fc^+/Fc obtained from CV titration data in (**A**). Conditions: 0.1 M $TBAPF_6$/MeCN; glassy carbon working electrode, glassy carbon counter electrode, Ag/AgCl pseudoreference electrode; 100 mV/s scan rate; referenced to internal ferrocene standard.

Table S2. Data from variable TFEOH concentration CV data with 2.5 mM BQ (**Figure S4**).

[TFEOH(M)]	$E_{1/2}$ (V vs. Fc^+/Fc)	ΔE_p (V)
0.0000	-0.888	0.0675
0.0132	-0.876	0.0675
0.0264	-0.867	0.0714
0.0396	-0.862	0.0725
0.0528	-0.855	0.0755
0.0660	-0.848	0.0756
0.0792	-0.839	0.0777
0.106	-0.825	0.0706
0.132	-0.812	0.0704
0.198	-0.783	0.0694

*Potential values in table correspond to data for the most positive BQ reduction potential, which has been characterize as a two-electron redox process when TFEOH is present as illustrated in coulometry experiments.

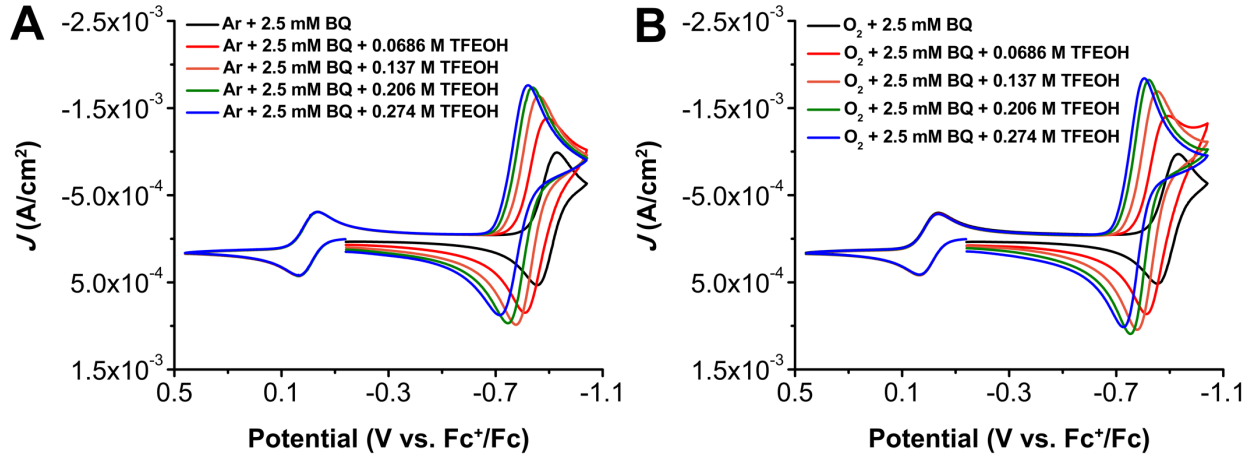

Figure S5. CVs with 2.5 mM BQ with variable TFEOH concentration under Ar (**A**) and O_2 (**B**) saturation conditions. Conditions: 0.1 M $TBAPF_6$/MeCN; glassy carbon working electrode, glassy carbon counter electrode, Ag/AgCl pseudoreference electrode; 100 mV/s scan rate; referenced to internal ferrocene standard.

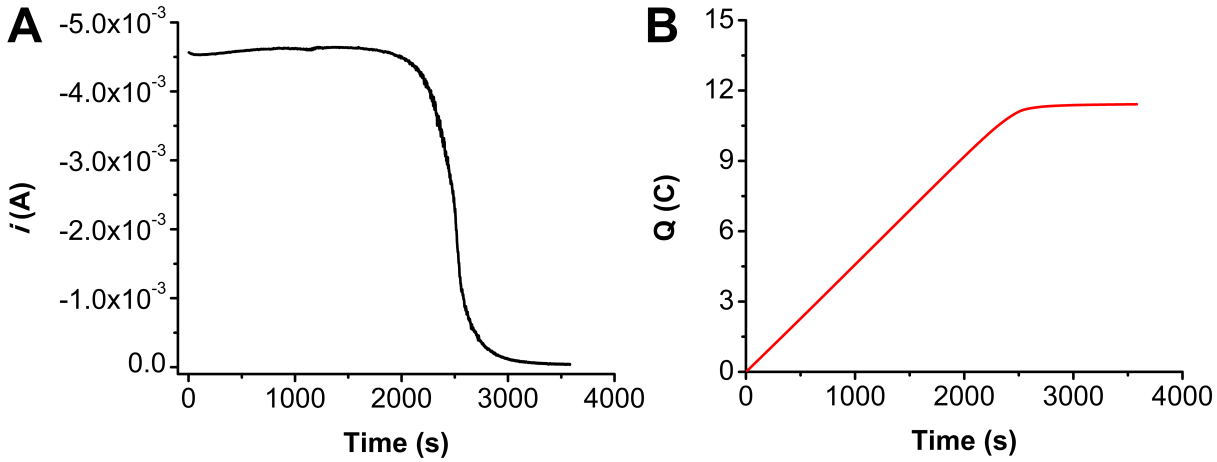

Figure S6. Coulometry experiment with 2.5 mM BQ and 1.37 M TFEOH in an MeCN solution under N_2 saturation conditions. Conditions: 0.1 M $TBAPF_6$/MeCN; Carbon cloth (Plain Carbon Cloth 1071 from FuelCellStore) working and counter electrodes; Ag/AgCl pseudoreference electrode. Applied potential of –1.1 V vs. Fc^+/Fc. The solution for this experiment contained 6.30 x 10^{-5} moles of BQ and a total of 11.42 C of charge was passed indicating 1.88 electrons were transferred.

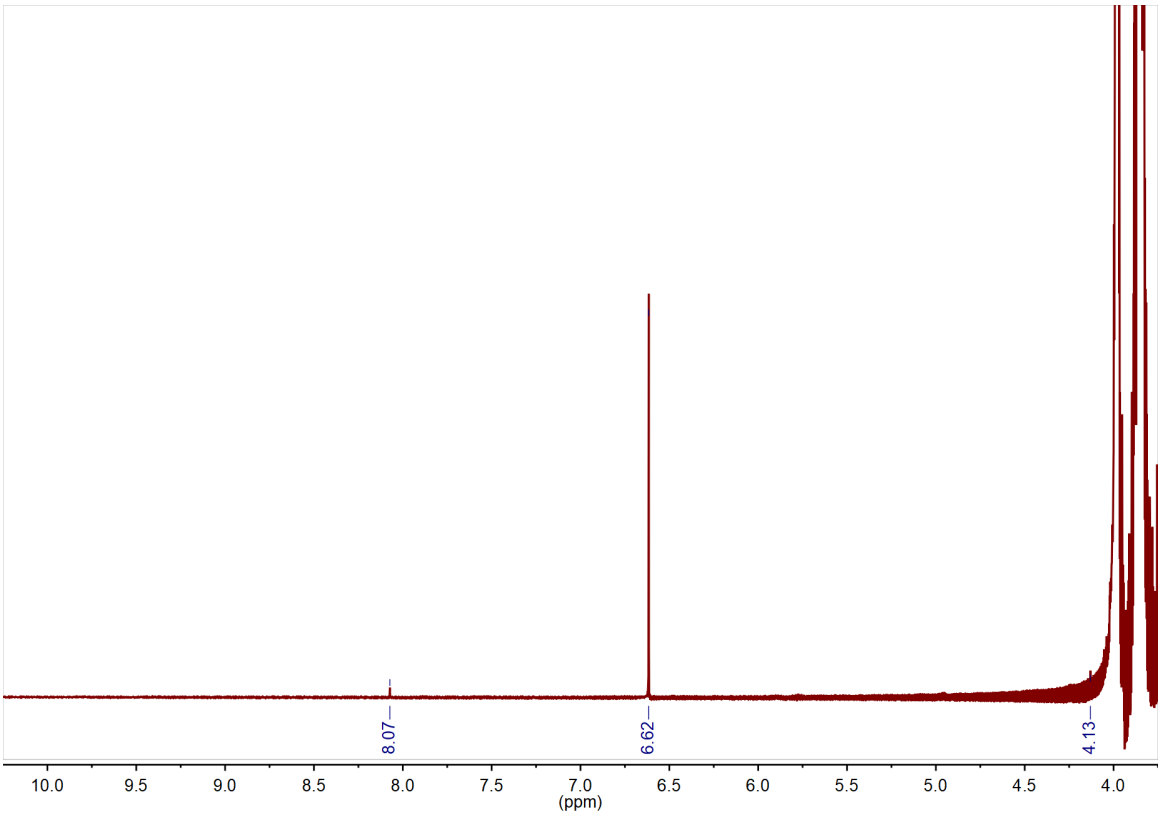

Figure S7. ^{1}H NMR taken after coulometry experiment with 2.5 mM BQ and 1.37 M TFEOH under an atmosphere of N_2. ^{1}H NMR solution was prepared from a 5:1 mixture of coulometry experiment solution and CD_3CN, respectively.

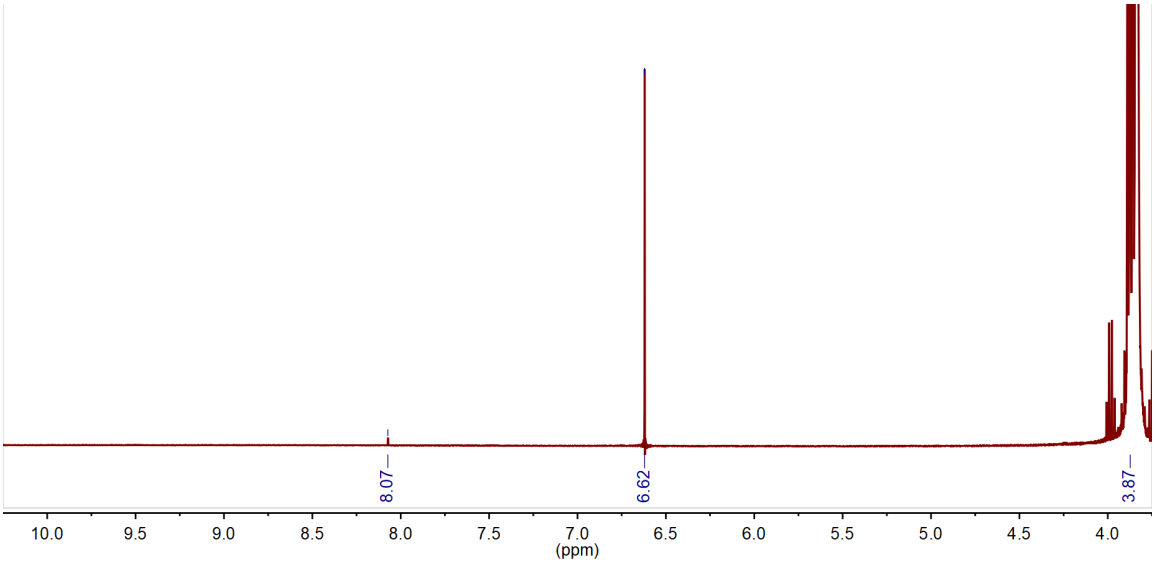

Figure S8. ^{1}H NMR taken of a solution with 2.5 mM H_2Q and 1.37 M TFEOH under an atmosphere of N_2. ^{1}H NMR solution was prepared from a 5:1 mixture of the MeCN experiment solution and CD_3CN, respectively.

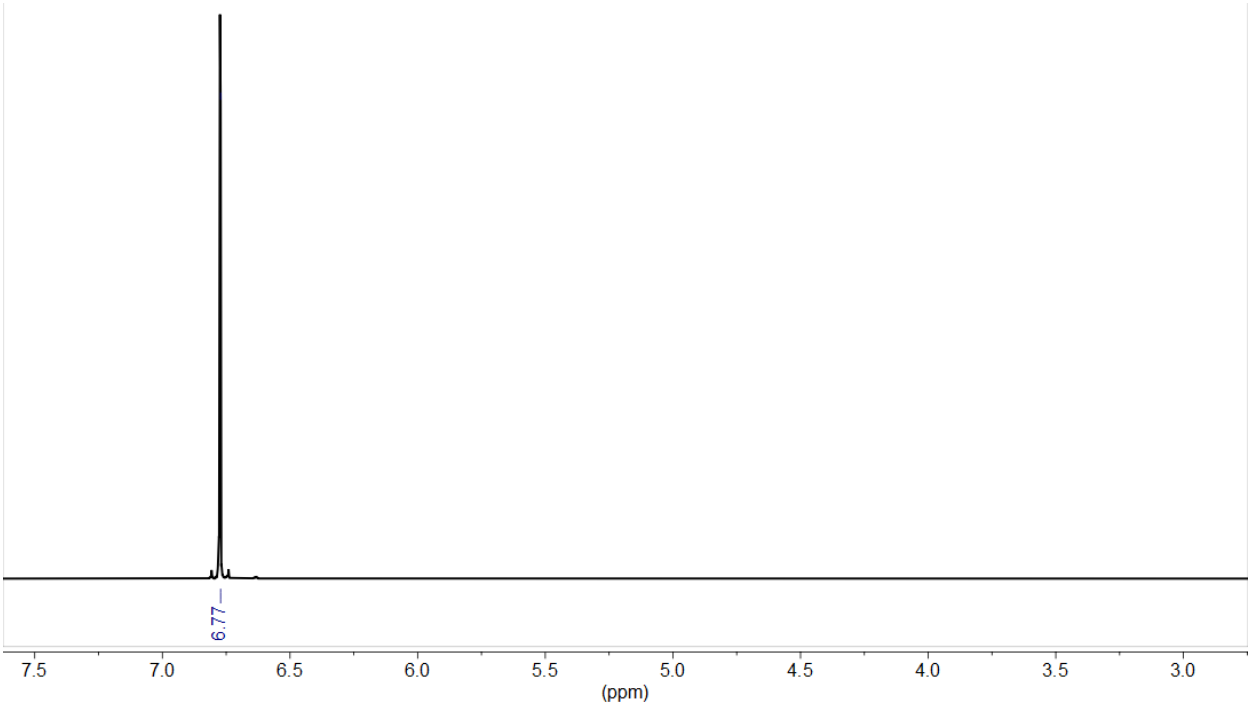

Figure S9. Control ^{1}H NMR of BQ in CD_3CN under an N_2 atmosphere.

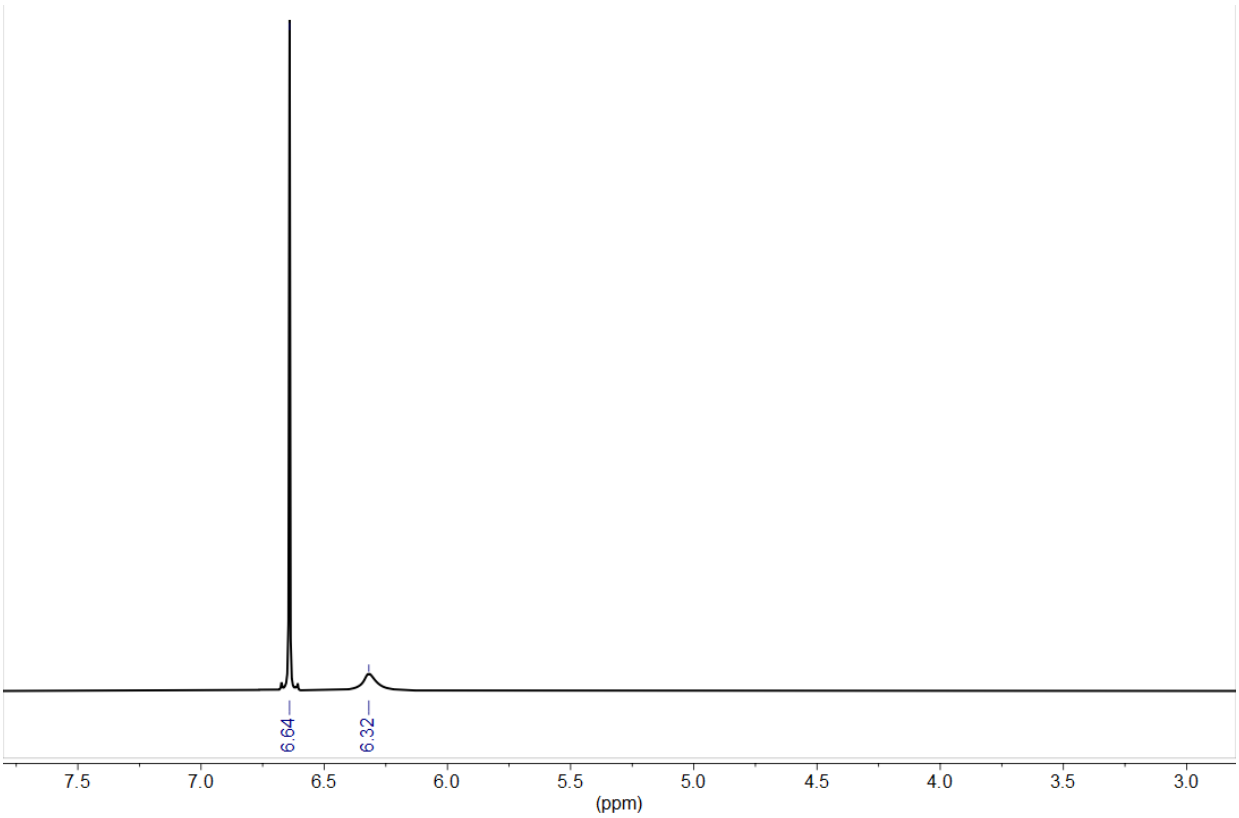

Figure S10. Control ^{1}H NMR of H_2Q in CD_3CN under an N_2 atmosphere.

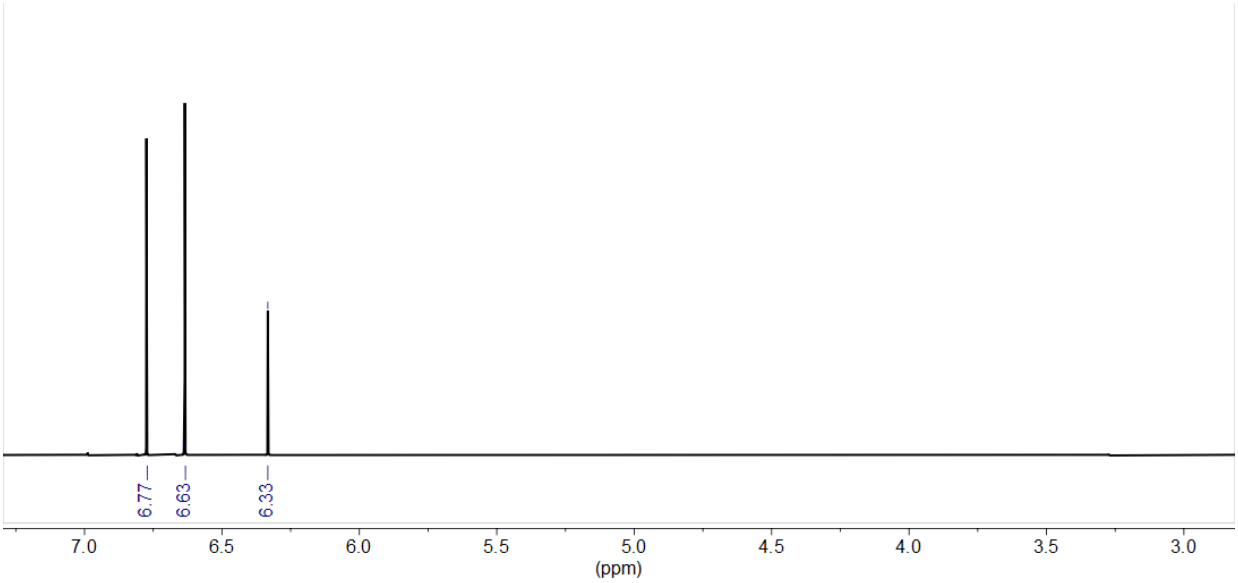

Figure S11. Control ^{1}H NMR of quinhydrone in CD_3CN under an N_2 atmosphere.

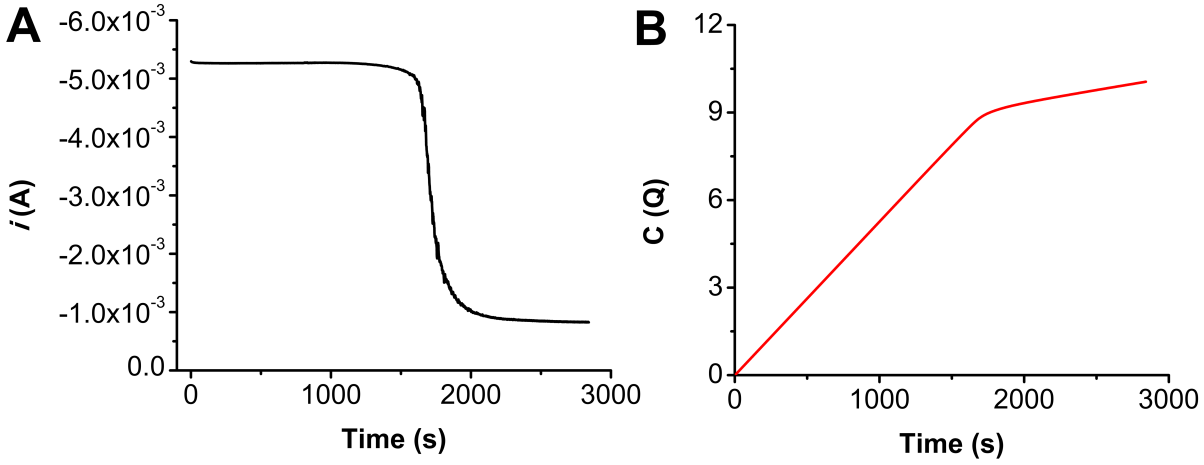

Figure S12. Coulometry experiment with 2.6 mM BQ and 1.37 M acetic acid in an MeCN solution under N_2 saturation conditions. Conditions: 0.1 M $TBAPF_6$/MeCN; Carbon cloth (Plain Carbon Cloth 1071 from FuelCellStore) working and counter electrodes; Ag/AgCl pseudoreference electrode. Applied potential of –1.1 V vs. Fc^+/Fc. The solution for this experiment contained 6.57 x 10^{-5} moles of BQ and a total of 10.06 C of charge was passed indicating 1.59 electrons were transferred.

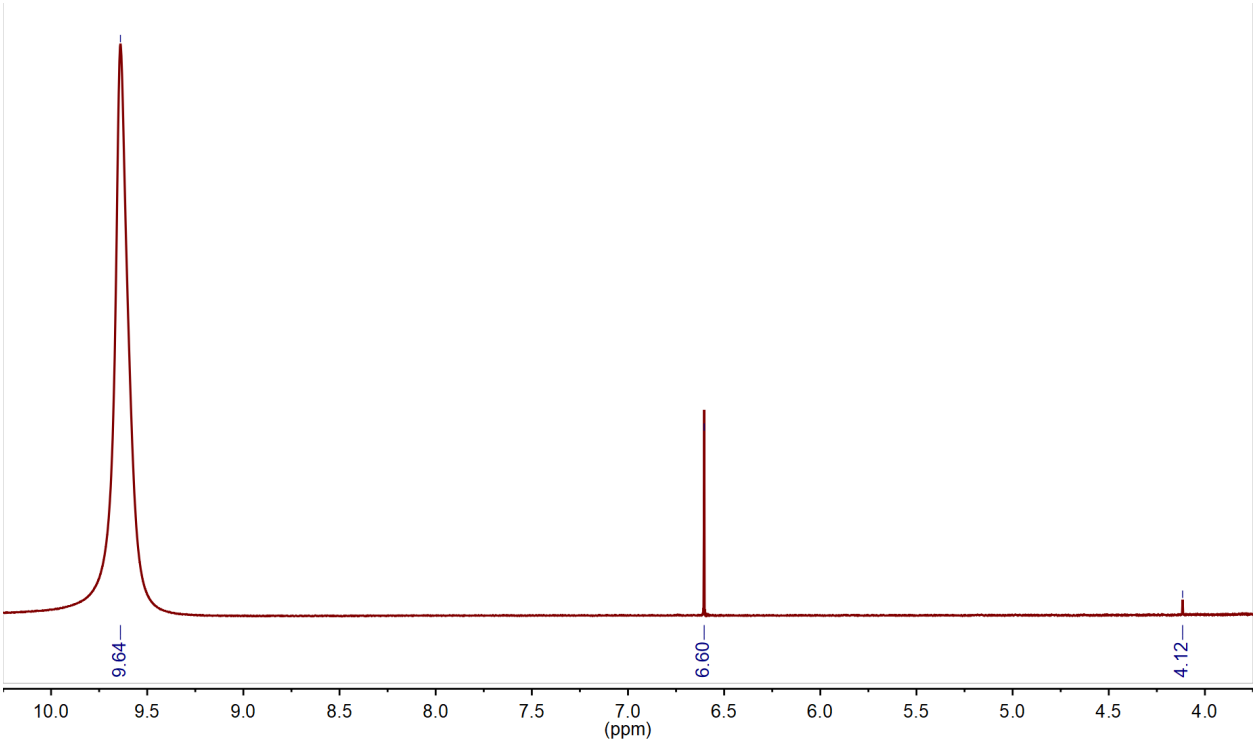

Figure S13. ^{1}H NMR taken after coulometry experiment with 2.6 mM BQ and 1.37 M acetic acid under an atmosphere of N_2. ^{1}H NMR solution was prepared from a 5:1 mixture of coulometry experiment solution and CD_3CN, respectively. The peak at 9.64 corresponds to acetic acid.

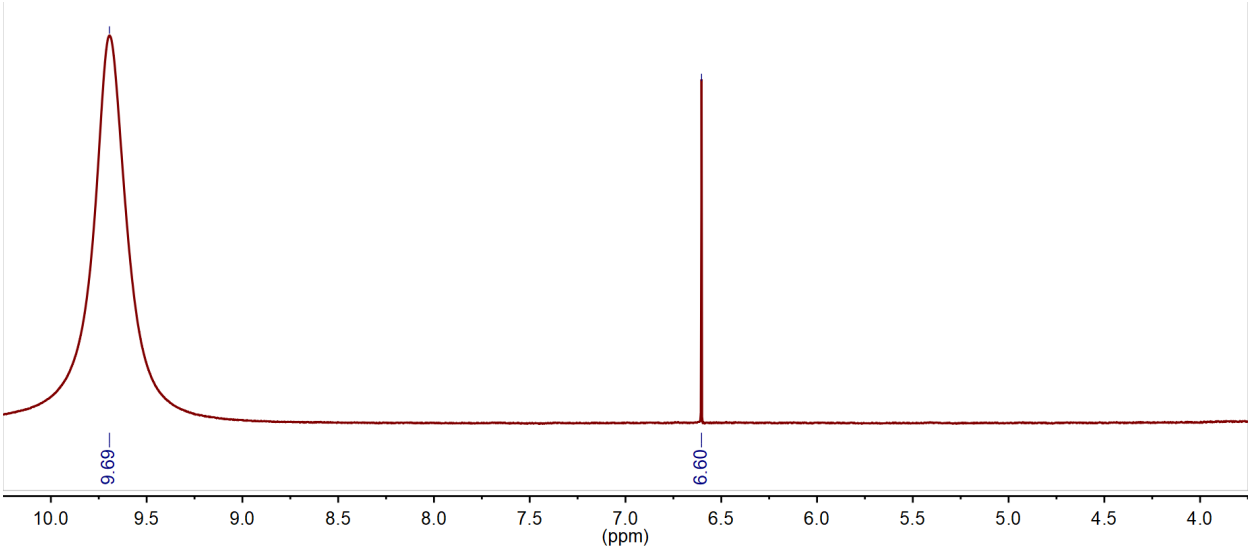

Figure S14. ^{1}H NMR taken of a solution with 2.5 mM H_2Q and 1.37 M acetic acid under an atmosphere of N_2. ^{1}H NMR solution was prepared from a 5:1 mixture of the MeCN experiment solution and CD_3CN, respectively. The peak at 9.69 is assigned to acetic acid.

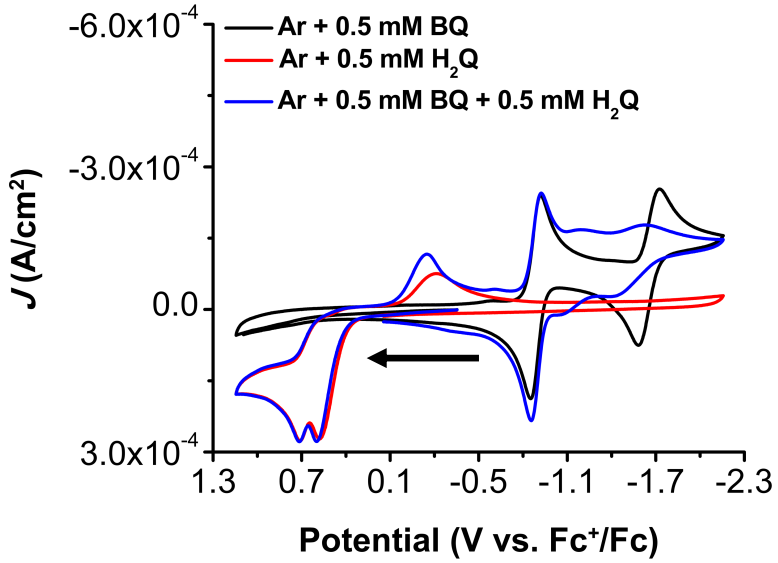

Figure S15. CV data comparing the individual responses of 0.5 mM H_2Q (red) and 0.5 mM BQ (black) relative to when they are both present in situ (blue). Conditions: 0.1 M $TBAPF_6$/MeCN; glassy carbon working electrode, glassy carbon counter electrode, Ag/AgCl pseudoreference electrode; 100 mV/s scan rate; referenced to internal ferrocene standard. Arrow designates the direction of the CV trace.

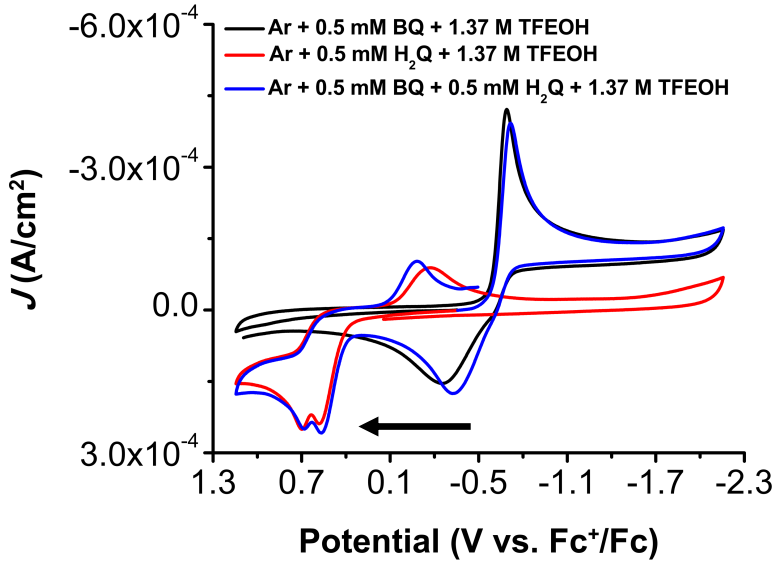

Figure S16. CV data with 1.37 M TFEOH comparing the individual responses of 0.5 mM H_2Q (red) and 0.5 mM BQ (black) relative to when they are both present in situ (blue). Conditions: 0.1 M $TBAPF_6$/MeCN; glassy carbon working electrode, glassy carbon counter electrode, Ag/AgCl pseudoreference electrode; 100 mV/s scan rate; referenced to internal ferrocene standard. Arrow designates the direction of the CV trace.

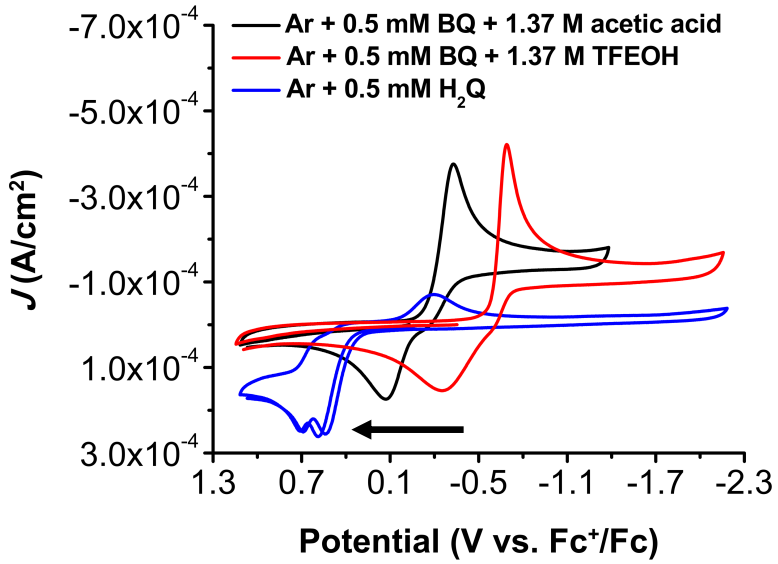

Figure S17. CV data under argon saturation conditions comparing 0.5 mM BQ with 1.37 M TFEOH (red) and 1.37 M acetic acid (black) with the redox response of 0.5 mM H_2Q under aprotic conditions (blue). Conditions: 0.1 M $TBAPF_6$/MeCN; glassy carbon working electrode, glassy carbon counter electrode, Ag/AgCl pseudoreference electrode; 100 mV/s scan rate; referenced to internal ferrocene standard. Arrow designates the direction of the CV trace. We note that the observed BQ reduction features do not align with H_2Q oxidation, with or without either TFEOH or acetic acid present. For acetic acid specifically, this has previously been attributed to non-covalent interactions between H_2Q generated in situ and the associated acetate ions.[1-2]

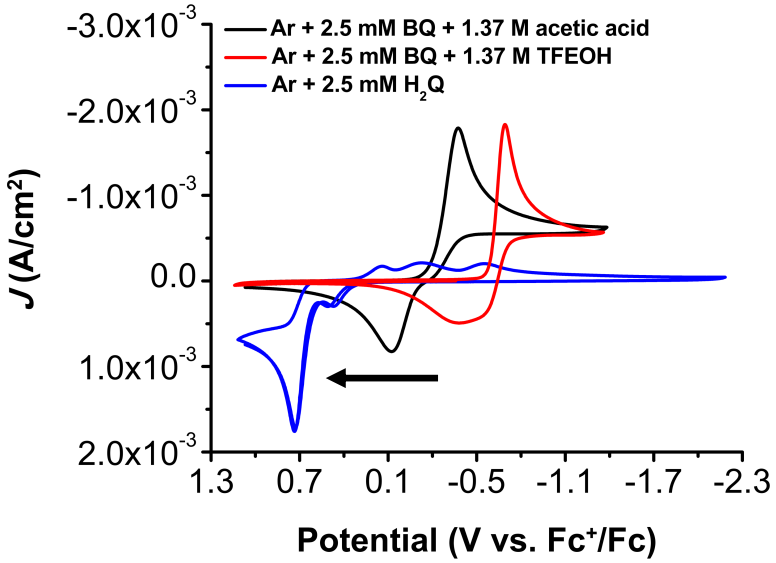

Figure S18. CV data under argon saturation conditions comparing 2.5 mM BQ with 1.37 M TFEOH (red) and 1.37 M acetic acid (black) with the redox response of 2.5 mM H_2Q under aprotic conditions (blue). Conditions: 0.1 M $TBAPF_6$/MeCN; glassy carbon working electrode, glassy carbon counter electrode, Ag/AgCl pseudoreference electrode; 100 mV/s scan rate; referenced to internal ferrocene standard. Arrow designates the direction of the CV trace. We note that the observed BQ reduction features do not align with H_2Q oxidation, with or without either TFEOH or acetic acid present. For acetic acid specifically, this has previously been attributed to non-covalent interactions between H_2Q generated in situ and the associated acetate ions.[1-2]

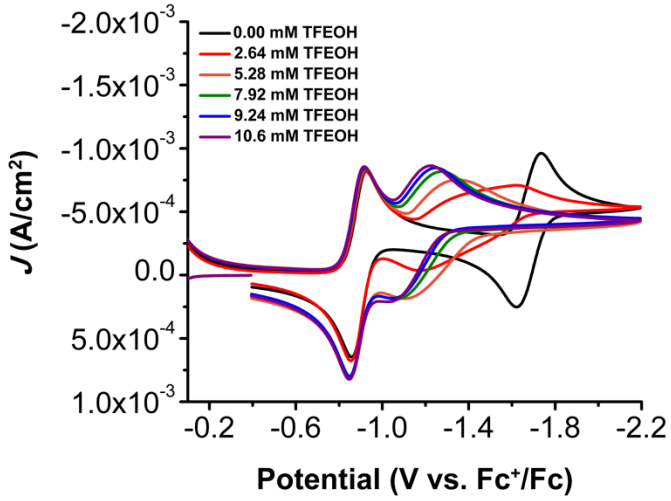

Figure S19. CVs of TFEOH titration with 2.5 mM BQ obtained under Ar saturation conditions focusing on the one-electron BQ reduction feature at –1.69 V vs. Fc^+/Fc obtained from CV titration data in. Conditions: 0.1 M $TBAPF_6$/MeCN; glassy carbon working electrode, glassy carbon counter electrode, Ag/AgCl pseudoreference electrode; 100 mV/s scan rate; referenced to internal ferrocene standard.

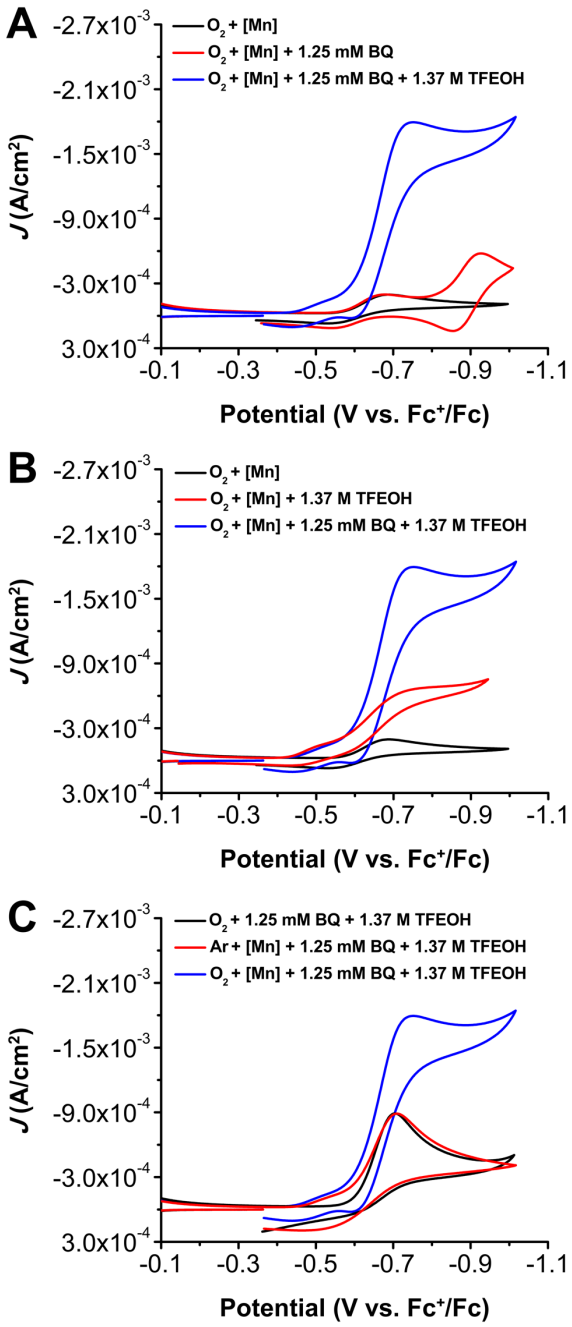

Figure S20. (**A**) CVs comparing 0.5 mM of Mn(^{tbu}dhbpy)Cl **1**, with 1.25 mM BQ both with (blue) and without (red) 1.37 M TFEOH under O_2 saturation conditions. (**B**) CVs comparing 0.5 mM of Mn(^{tbu}dhbpy)Cl **1**, with 1.37 M TFEOH both with (blue) and without (red) 1.25 mM BQ. (**C**) CVs comparing 0.5 mM Mn(^{tbu}dhbpy)Cl **1**, with 1.37 M TFEOH and 0.125 mM BQ under Ar (red) and O_2 (blue) saturation conditions compared to a control CV in the absence of Mn(^{tbu}dhbpy)Cl **1** (black). Conditions: 0.1 M $TBAPF_6$/MeCN; glassy carbon working electrode, glassy carbon counter electrode, Ag/AgCl pseudoreference electrode; 100 mV/s scan rate; referenced to internal ferrocene standard.

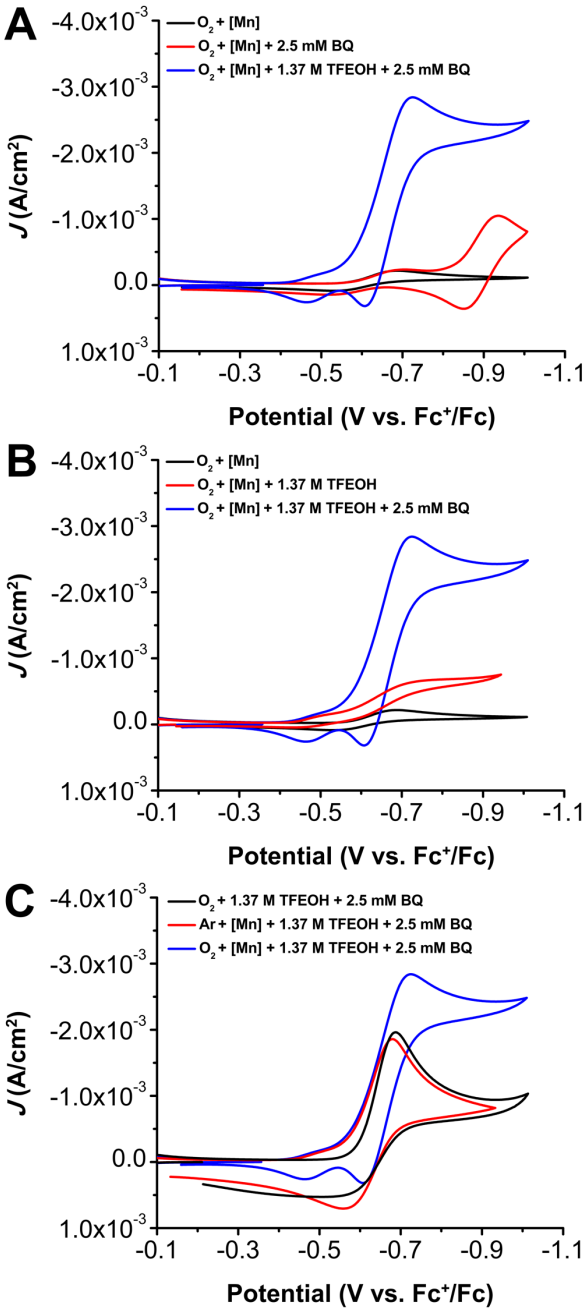

Figure S21. (**A**) CVs comparing 0.5 mM of Mn(^{tbu}dhbpy)Cl **1**, with 2.5 mM BQ both with (blue) and without (red) 1.37 M TFEOH under O_2 saturation conditions. (**B**) CVs comparing 0.5 mM of Mn(^{tbu}dhbpy)Cl **1**, with 1.37 M TFEOH both with (blue) and without (red) 2.5 mM BQ. (**C**) CVs comparing 0.5 mM Mn(^{tbu}dhbpy)Cl **1**, with 1.37 M TFEOH and 2.5 mM BQ under Ar (red) and O_2 (blue) saturation conditions compared to a control CV in the absence of Mn(^{tbu}dhbpy)Cl **1** (black). Conditions: 0.1 M $TBAPF_6$/MeCN; glassy carbon working electrode, glassy carbon counter electrode, Ag/AgCl pseudoreference electrode; 100 mV/s scan rate; referenced to internal ferrocene standard.

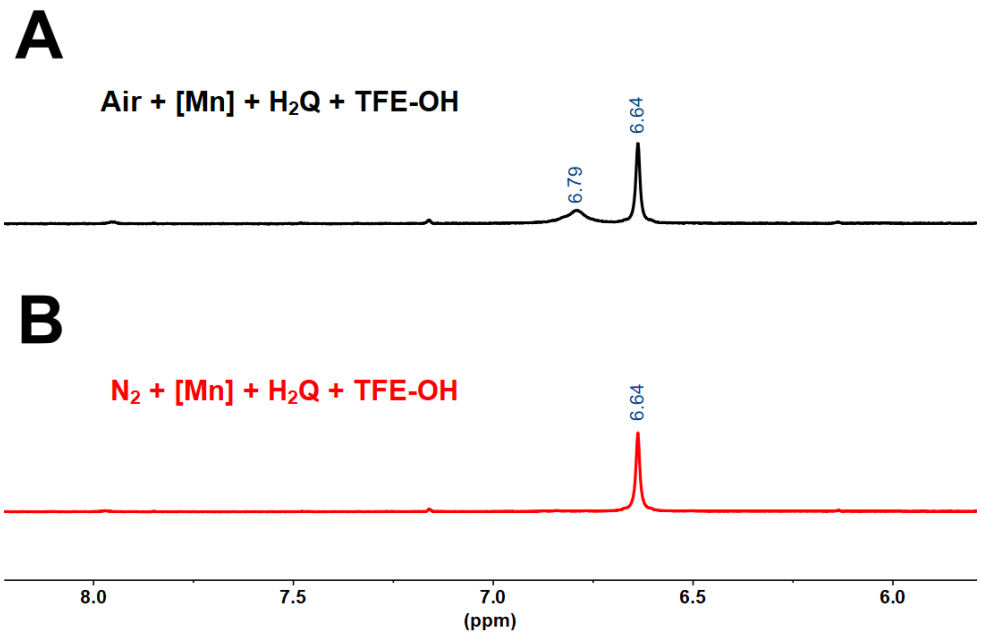

Figure S22. Overlay of ^{1}H NMR aromatic region from experiment with 2.5 mM H_2Q, 0.274 M TFEOH, and 0.5 mM Mn(^{tbu}dhbpy)Cl **1** in CD_3CN under an atmosphere of N_2 (B, red) versus an atmosphere of air (A, black). [Mn] = Mn(^{tbu}dhbpy)Cl **1**.

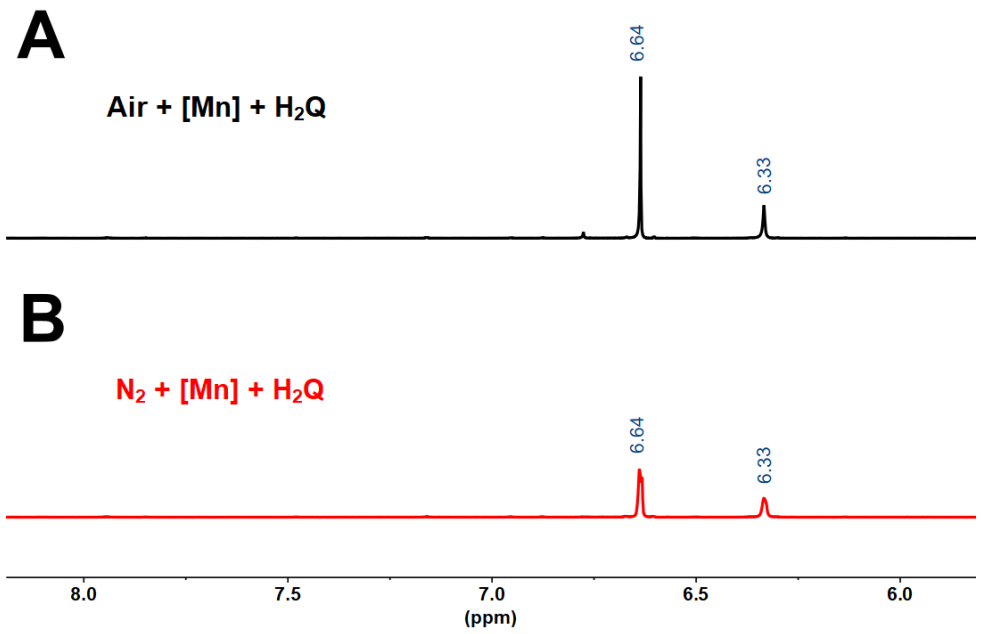

Figure S23. Overlay of ^{1}H NMR aromatic region from experiment with 2.5 mM H_2Q and 0.5 mM Mn(^{tbu}dhbpy)Cl **1** in CD_3CN under an atmosphere of N_2 (B, red) versus an atmosphere of air (A, black). [Mn] = Mn(^{tbu}dhbpy)Cl **1**.

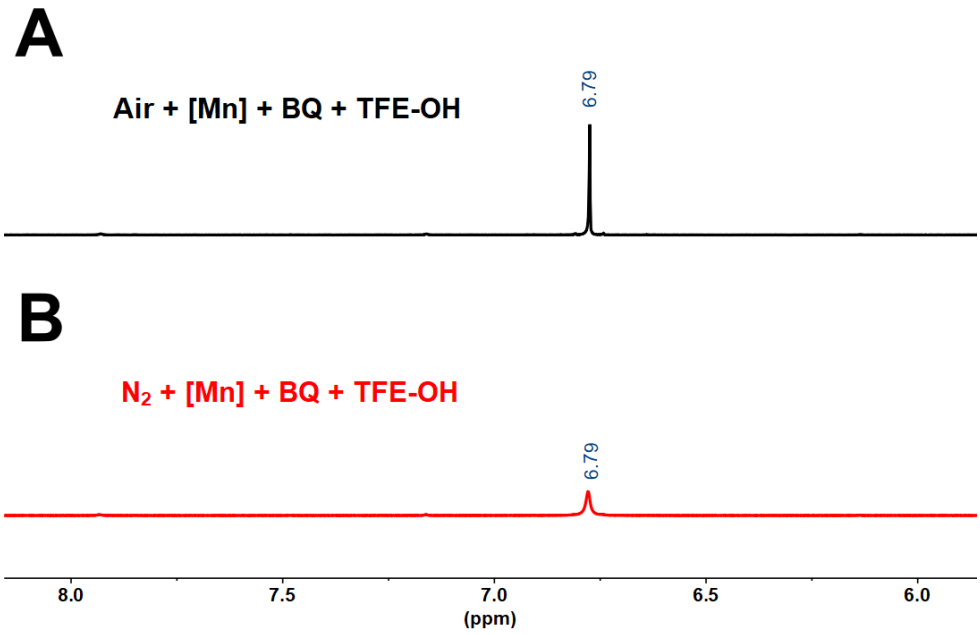

Figure S24. Overlay of ^{1}H NMR aromatic region from experiment with 2.5 mM BQ, 0.274 M TFEOH, and 0.5 mM Mn(^{tbu}dhbpy)Cl **1** in CD_3CN under an atmosphere of N_2 (B, red) versus an atmosphere of air (A, black). [Mn] = Mn(^{tbu}dhbpy)Cl **1**.

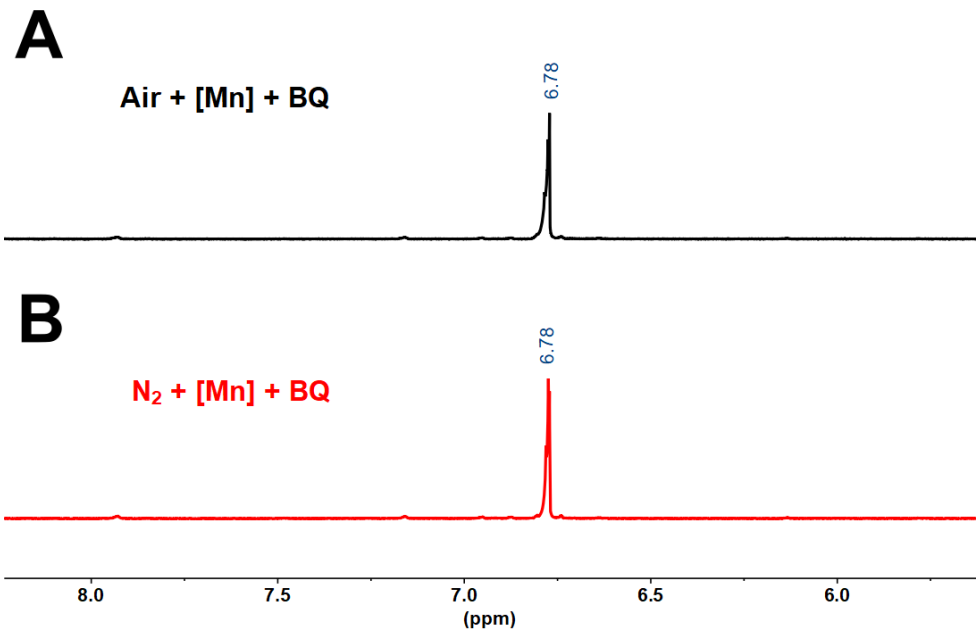

Figure S25. Overlay of ^{1}H NMR aromatic region from experiment with 2.5 mM BQ and 0.5 mM Mn(^{tbu}dhbpy)Cl **1** in CD_3CN under an atmosphere of N_2 (B, red) versus an atmosphere of air (A, black). [Mn] = Mn(^{tbu}dhbpy)Cl **1**.

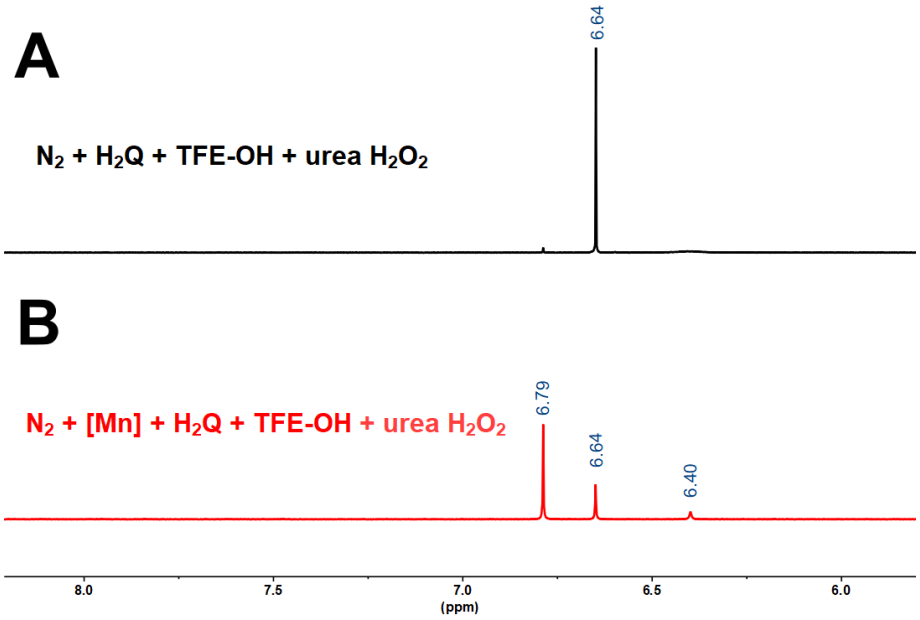

Figure S26. Overlay of ^{1}H NMR aromatic region from experiment with 0.5 mM H_2Q, 0.5 mM urea•H_2O_2, 0.274 M TFEOH in CD_3CN under an N_2 atmosphere with 0.5 mM Mn(^{tbu}dhbpy)Cl **1** present (B, red) and in the absence of Mn(^{tbu}dhbpy)Cl **1** (A, black). [Mn] = Mn(^{tbu}dhbpy)Cl **1**.

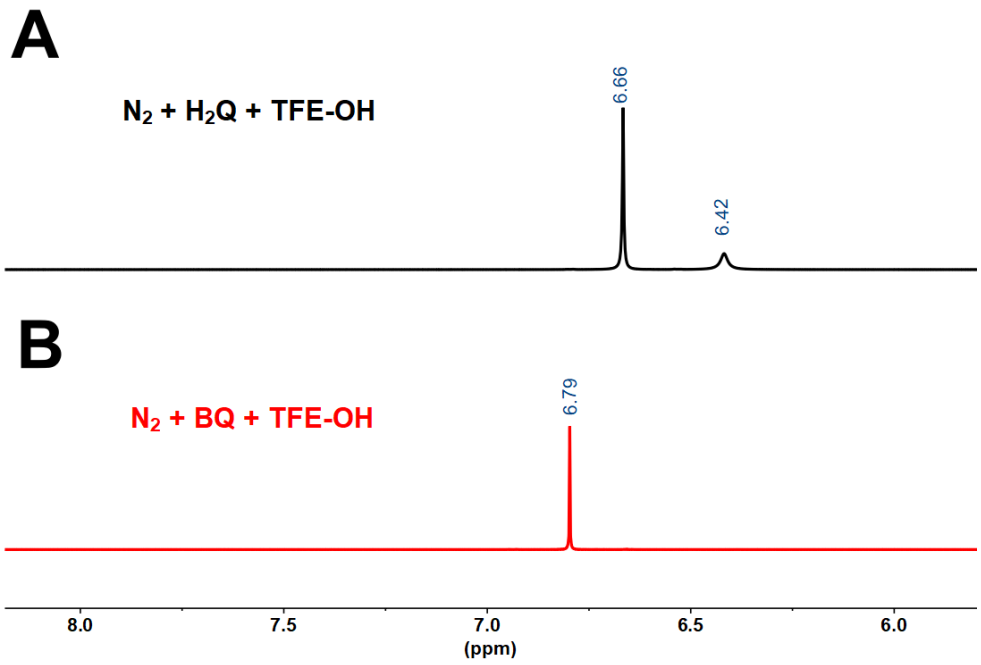

Figure S27. Aromatic region of control ^{1}H NMRs of 0.274 M TFEOH with 2.5 mM BQ (A, black) versus 2.5 mM H_2Q (B, red) in CD_3CN under an N_2 atmosphere.

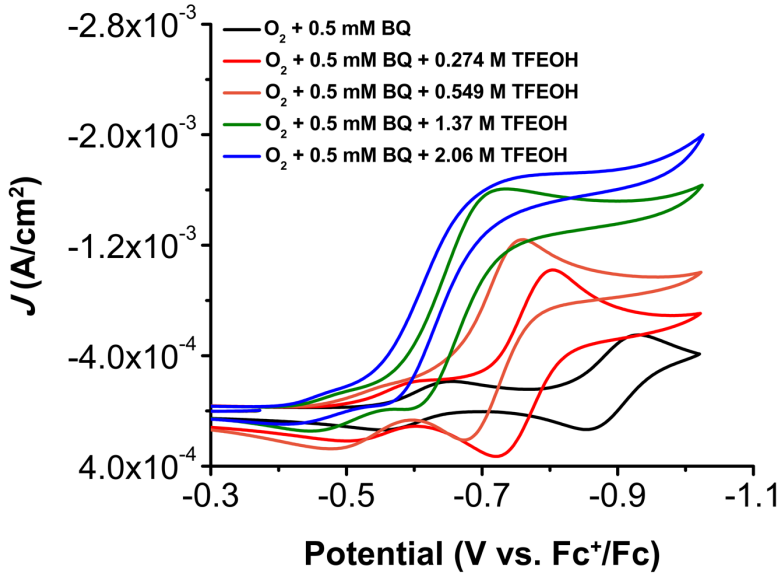

Figure S28. CVs of 0.5 mM Mn(^{tbu}dhbpy)Cl **1**, and 0.5 mM BQ obtained under O_2 saturation conditions with variable TFEOH concentration. Conditions: 0.1 M $TBAPF_6$/MeCN; glassy carbon working electrode, glassy carbon counter electrode, Ag/AgCl pseudoreference electrode; 100 mV/s scan rate; referenced to internal ferrocene standard.

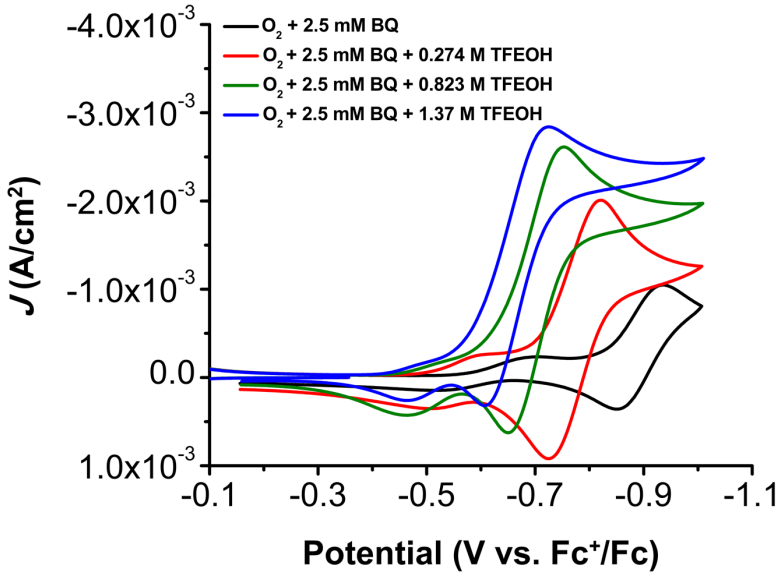

Figure S29. CVs of 0.5 mM Mn(^{tbu}dhbpy)Cl **1**, and 2.5 mM BQ obtained under O_2 saturation conditions with variable TFEOH concentration. Conditions: 0.1 M $TBAPF_6$/MeCN; glassy carbon working electrode, glassy carbon counter electrode, Ag/AgCl pseudoreference electrode; 100 mV/s scan rate; referenced to internal ferrocene standard.

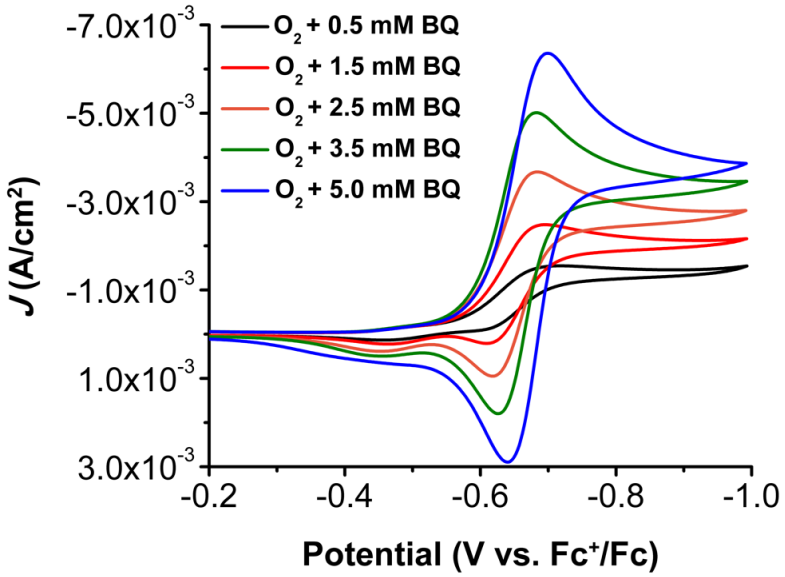

Figure S30. CVs of 0.5 mM Mn(^{tbu}dhbpy)Cl **1**, and 1.37 M TFEOH obtained under O_2 saturation conditions with variable BQ concentration. Conditions: 0.1 M $TBAPF_6$/MeCN; glassy carbon working electrode, glassy carbon counter electrode, Ag/AgCl pseudoreference electrode; 100 mV/s scan rate; referenced to internal ferrocene standard.

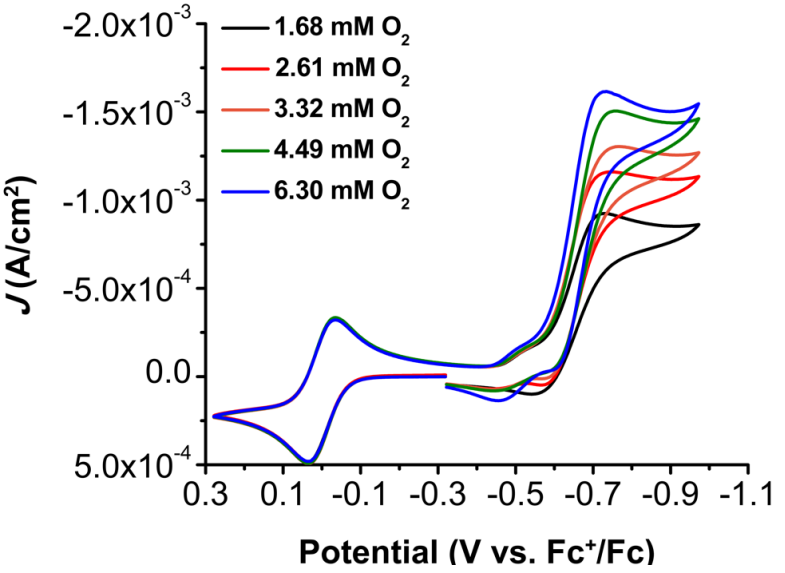

Figure S31. CVs of 0.5 mM Mn(^{tbu}dhbpy)Cl **1**, 0.5 mM BQ, and 1.37 M TFEOH with variable O_2 concentration. Conditions: 0.1 M $TBAPF_6$/MeCN; glassy carbon working electrode, glassy carbon counter electrode, Ag/AgCl pseudoreference electrode; 100 mV/s scan rate; referenced to internal ferrocene standard.

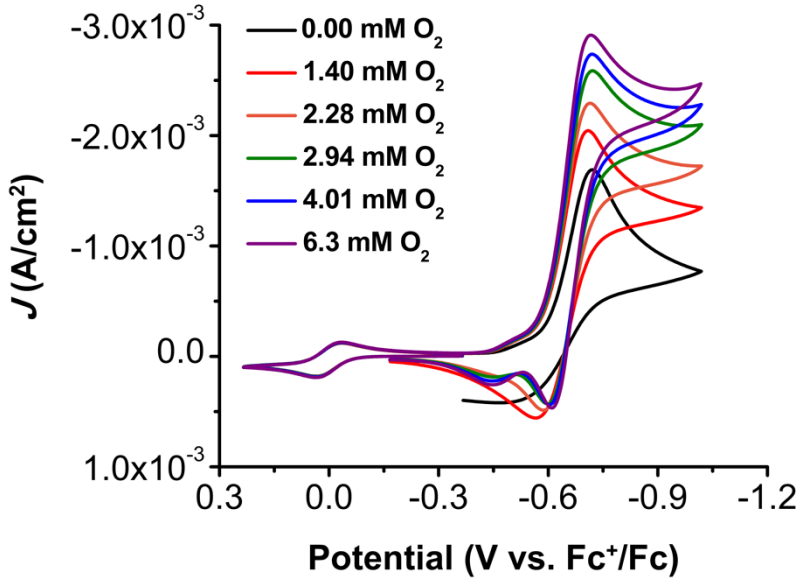

Figure S32. CVs of 0.5 mM Mn(^{tbu}dhbpy)Cl **1**, 2.5 mM BQ, and 1.37 M TFEOH with variable O_2 concentration. Conditions: 0.1 M $TBAPF_6$/MeCN; glassy carbon working electrode, glassy carbon counter electrode, Ag/AgCl pseudoreference electrode; 100 mV/s scan rate; referenced to internal ferrocene standard.

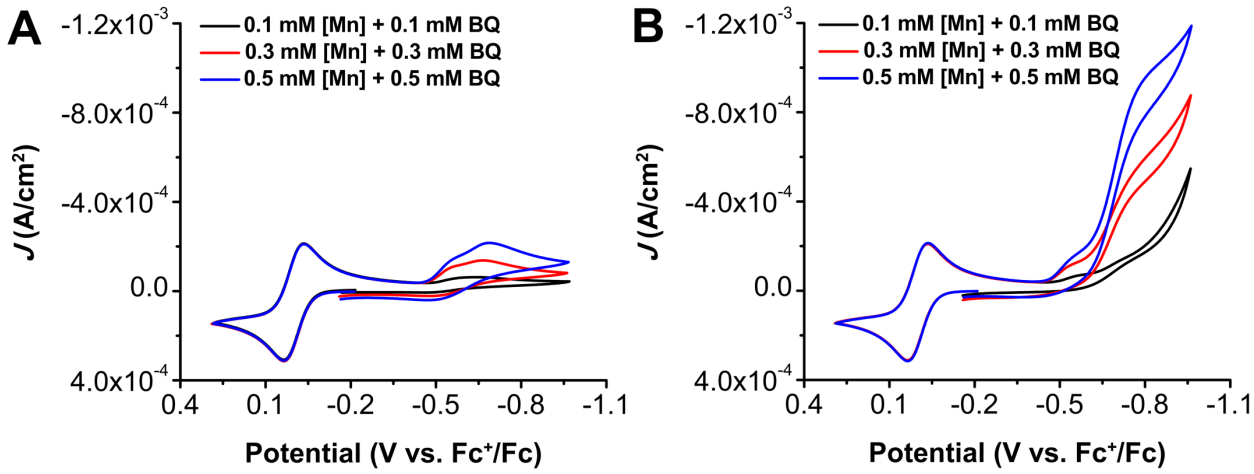

Figure S33. CVs with 1.37 M TFEOH under Ar (**A**) and O_2 (**B**) saturation conditions with variable Mn(^{tbu}dhbpy)Cl **1** and BQ concentration. Conditions: 0.1 M $TBAPF_6$/MeCN; glassy carbon working electrode, glassy carbon counter electrode, Ag/AgCl pseudoreference electrode; 100 mV/s scan rate; referenced to internal ferrocene standard.

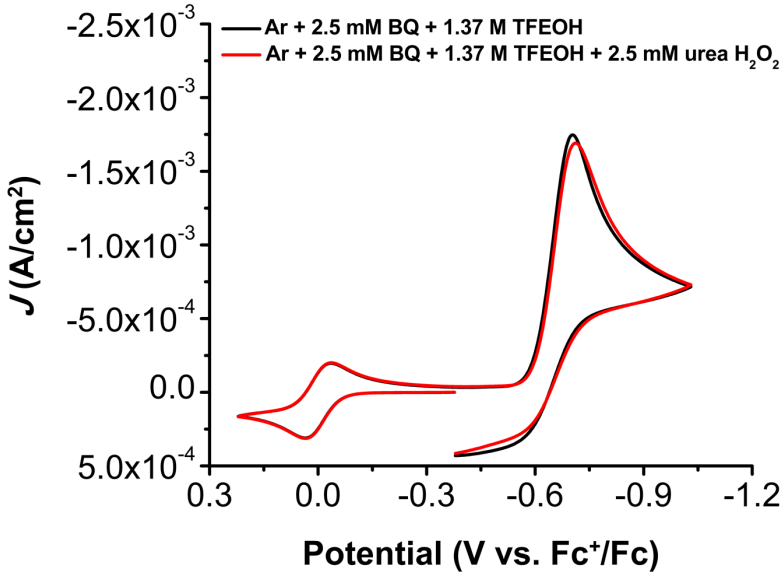

Figure S34. Control CVs of 2.5 mM BQ with 1.37 M TFEOH and 2.5 mM urea H_2O_2 under Ar saturation conditions to illustrate that no significant reactivity occurs between BQ and free H_2O_2 in the presence of a proton source. Conditions: 0.1 M $TBAPF_6$/MeCN; glassy carbon working electrode, glassy carbon counter electrode, Ag/AgCl pseudoreference electrode; 100 mV/s scan rate; referenced to internal ferrocene standard.

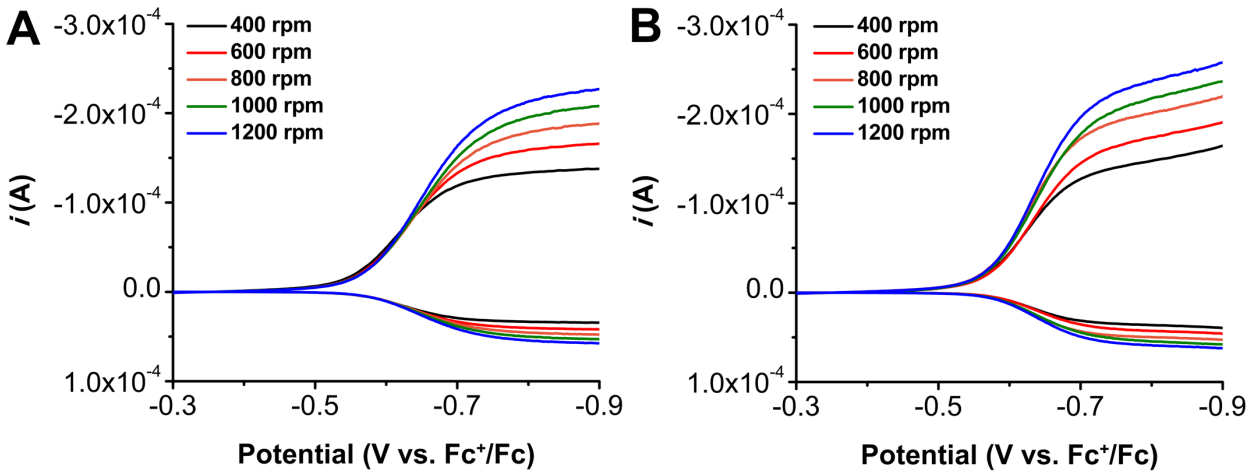

Figure S35. Linear Sweep Voltammograms of RRDE experiment with 0.5 mM BQ and 1.37 M TFEOH at various rotation rates under Ar (**A**) and O_2 (**B**) saturation conditions; ring potential = 0.85 V vs Fc^+/Fc. Conditions: glassy carbon working electrode/Pt ring working electrode, glassy carbon rod counter electrode, Ag/AgCl pseudoreference electrode; scan rate 0.02 V/s.

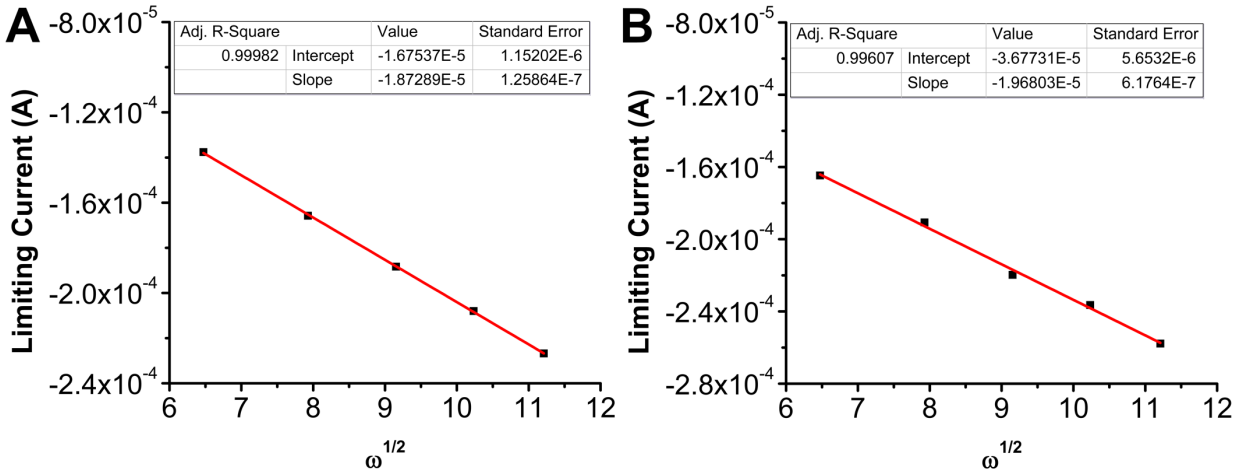

Figure S36. Levich plots from data obtained from Linear Sweep Voltammograms of BQ (0.5 mM) by RRDE with 1.37 M TFE under Ar (**A**) and O_2 (**B**) saturation conditions at various rotation rates; ring potential = 0.85 V vs Fc^+/Fc.

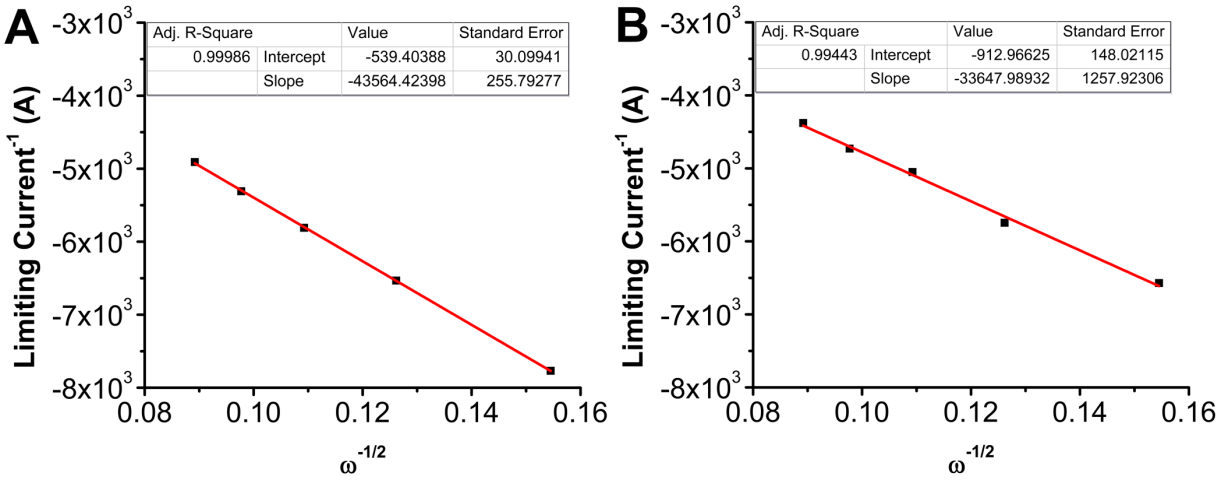

Figure S37. Koutecky-Levich plots from data obtained from Linear Sweep Voltammograms of BQ (0.5 mM) by RRDE with 1.37 M TFE under Ar (**A**) and O_2 (**B**) saturation conditions at various rotation rates; ring potential = 0.85 V vs Fc^+/Fc.

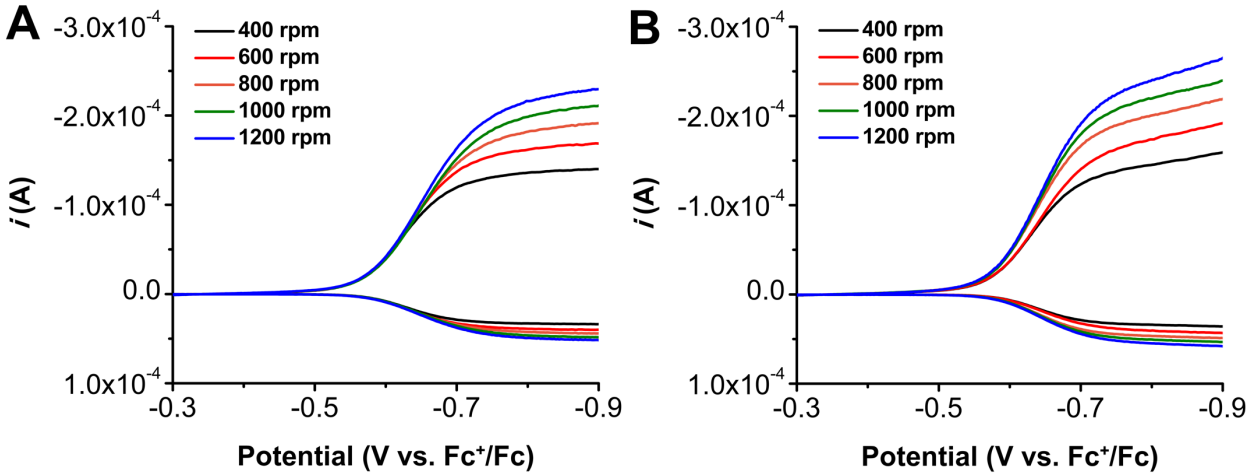

Figure S38. Linear Sweep Voltammograms of RRDE experiment with 0.5 mM BQ and 1.37 M TFEOH at various rotation rates under Ar (**A**) and O_2 (**B**) saturation conditions; ring potential = 0.4 V vs Fc^+/Fc. Conditions: glassy carbon working electrode/Pt ring working electrode, glassy carbon rod counter electrode, Ag/AgCl pseudoreference electrode; scan rate 0.02 V/s.

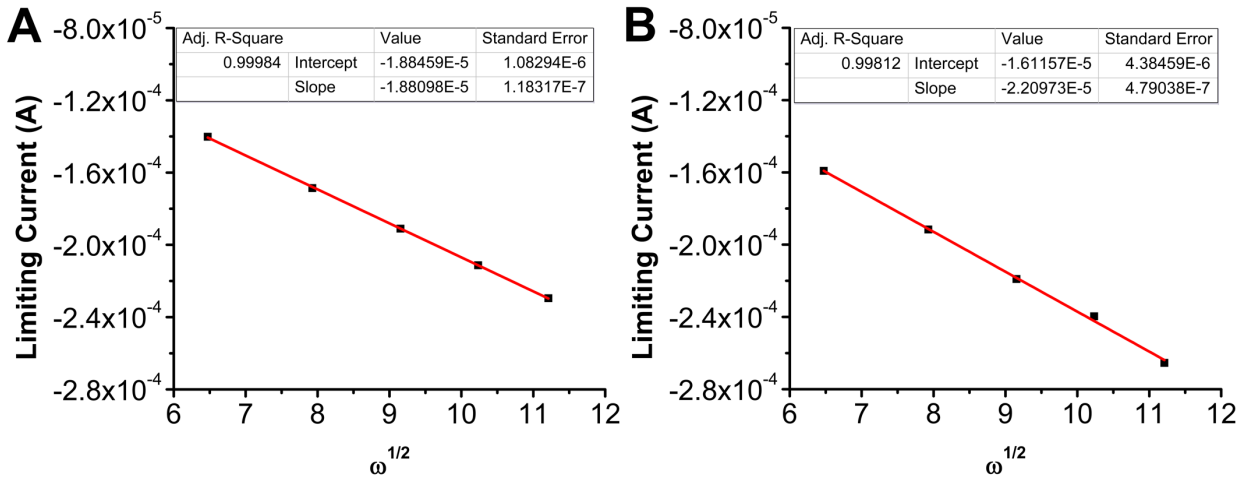

Figure S39. Levich plots from data obtained from Linear Sweep Voltammograms of BQ (0.5 mM) by RRDE with 1.37 M TFE under Ar (**A**) and O_2 (**B**) saturation conditions at various rotation rates; ring potential = 0.4 V vs Fc^+/Fc.

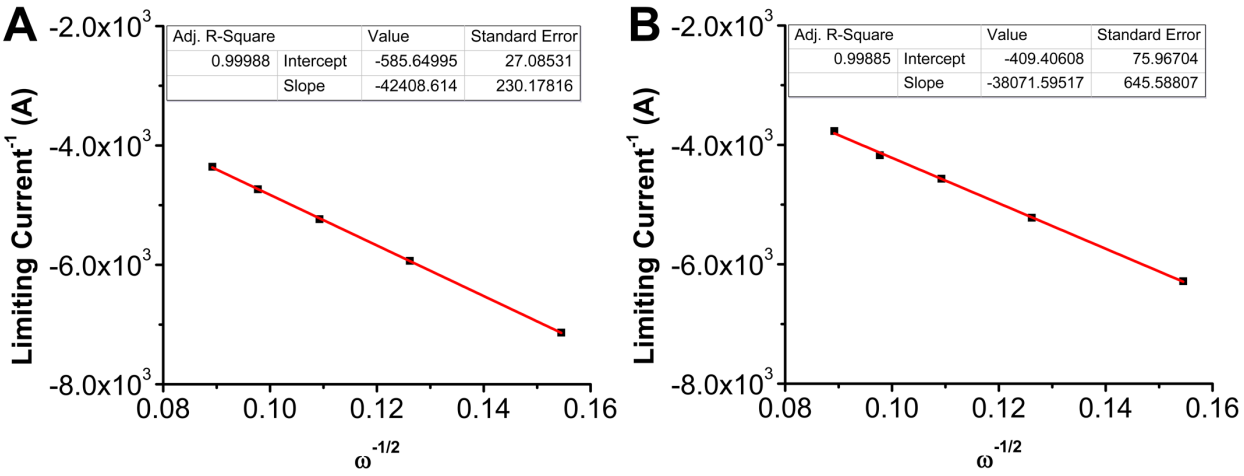

Figure S40. Koutecky-Levich plots from data obtained from Linear Sweep Voltammograms of BQ (0.5 mM) by RRDE with 1.37 M TFE under Ar (**A**) and O_2 (**B**) saturation conditions at various rotation rates; ring potential = 0.4 V vs Fc^+/Fc.

Table S3. Summary of O_2 Reduction Product Ananlysis Quantified from RRDE Experiments

Conditions	% Selectivity for H_2O_2	% Selectivity for H_2O
0.5 mM BQ + TFEOH[a]	10 (±23)%	n/a
0.5 mM Mn + TFEOH[b]	68 (±13)%	32 (±13)%
0.5 mM Mn + 0.5 mM BQ + TFEOH[c]	69 (±0.3)%	31 (±0.3)%
0.5 mM Mn + 1.25 mM BQ + TFEOH[c]	55 (±4)%	45 (±4)%
0.5 mM Mn + 2.5 mM BQ + TFEOH[c]	96 (±0.5)%	4 (±0.5)%

*-[a] denotes where selectivity was calculated across all rotation rates. -[b] denotes where selectivity was calculated at catalyst $E_{1/2}$ (-0.63 V vs. Fc^+/Fc). -[c] denotes where selectivity was calculated at the rotation rate of 400 rpm

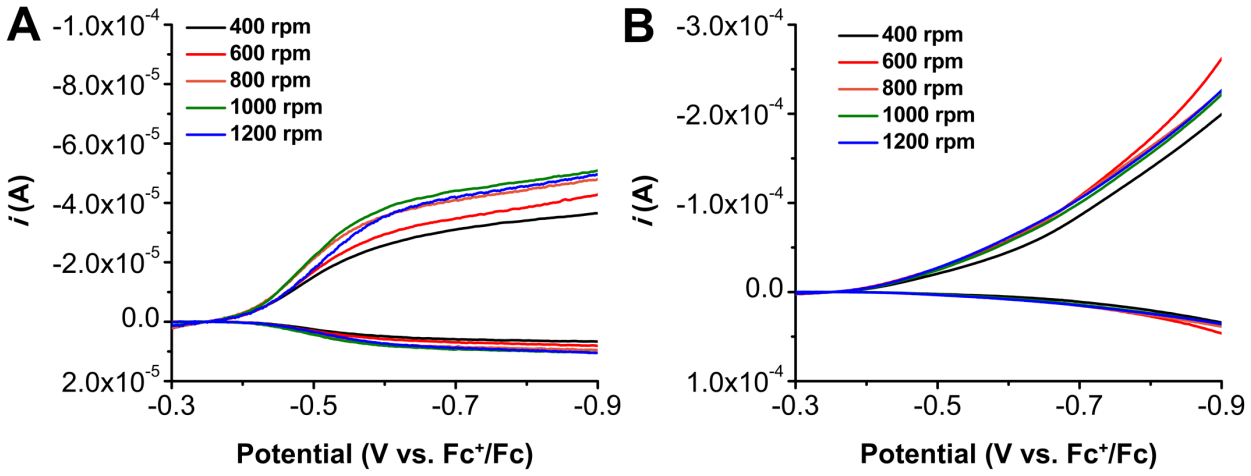

Figure S41. Linear Sweep Voltammograms of RRDE experiment with 0.5 mM Mn(^{tbu}dhbpy)Cl **1** and 1.37 M TFEOH at various rotation rates under Ar (**A**) and O_2 (**B**) saturation conditions; ring potential = 0.85 V vs Fc^+/Fc. Conditions: glassy carbon working electrode/Pt ring working electrode, glassy carbon rod counter electrode, Ag/AgCl pseudoreference electrode; scan rate 0.02 V/s.

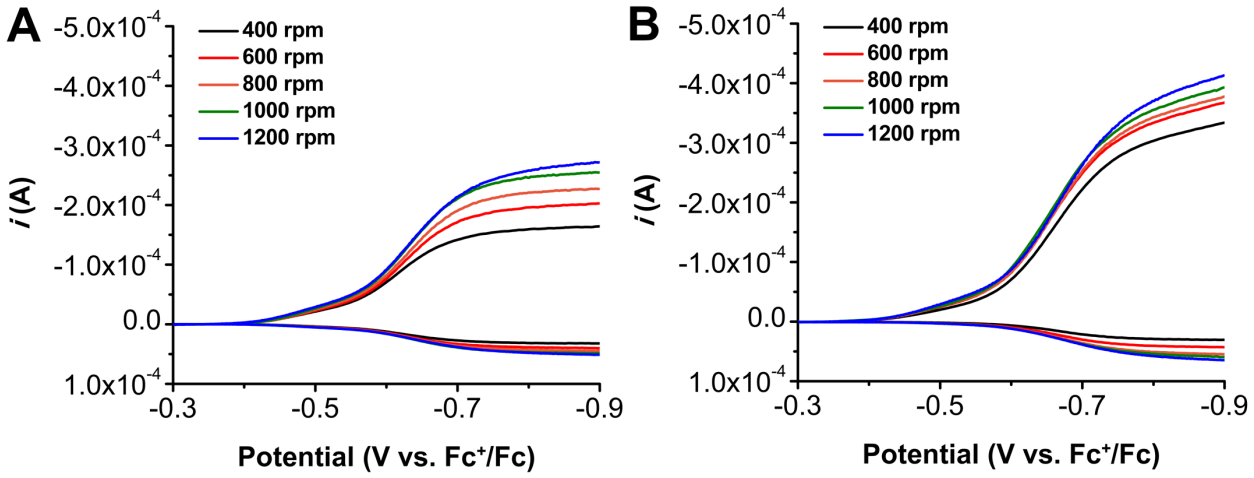

Figure S42. Linear Sweep Voltammograms of RRDE experiment with 0.5 mM Mn(^{tbu}dhbpy)Cl **1**, 0.5 mM BQ and 1.37 M TFEOH at various rotation rates under Ar (**A**) and O_2 (**B**) saturation conditions; ring potential = 0.4 V vs Fc^+/Fc. Conditions: glassy carbon working electrode/Pt ring working electrode, glassy carbon rod counter electrode, Ag/AgCl pseudoreference electrode; scan rate 0.02 V/s.

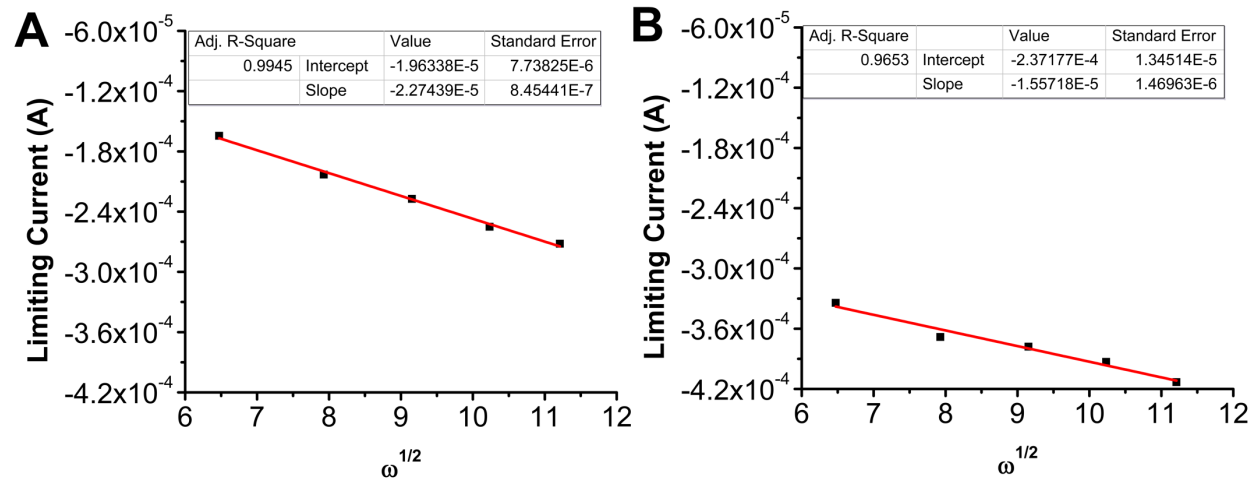

Figure S43. Levich plots from data obtained from Linear Sweep Voltammograms of 0.5 mM Mn(^{tbu}dhbpy)Cl **1** and 0.5 mM BQ by RRDE with 1.37 M TFE under Ar (**A**) and O_2 (**B**) saturation conditions at various rotation rates; ring potential = 0.4 V vs Fc^+/Fc.

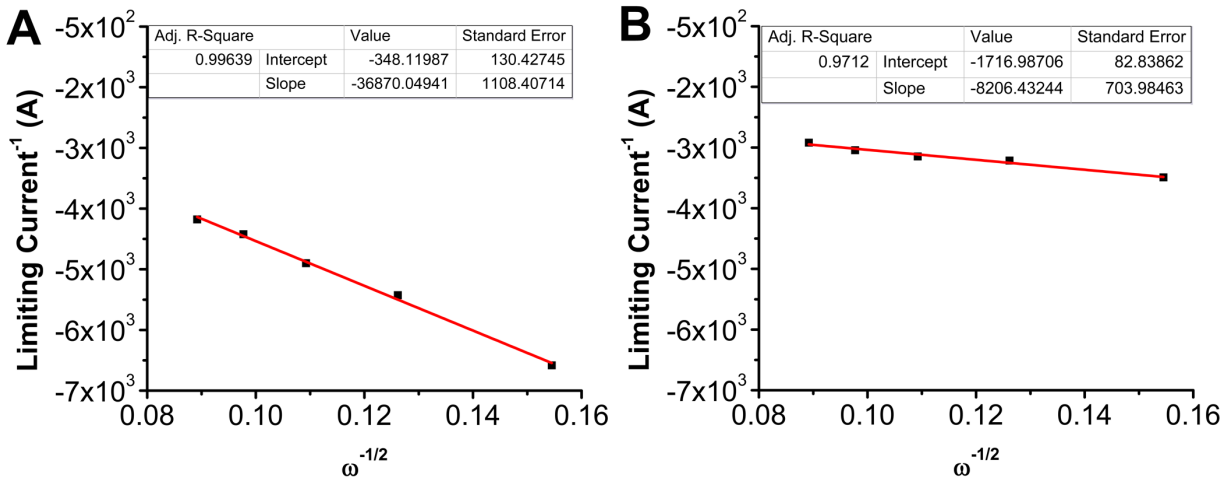

Figure S44. Koutecky-Levich plots from data obtained from Linear Sweep Voltammograms of 0.5 mM Mn(^{tbu}dhbpy)Cl **1** and 0.5 mM BQ by RRDE with 1.37 M TFE under Ar (**A**) and O_2 (**B**) saturation conditions at various rotation rates; ring potential = 0.4 V vs Fc^+/Fc.

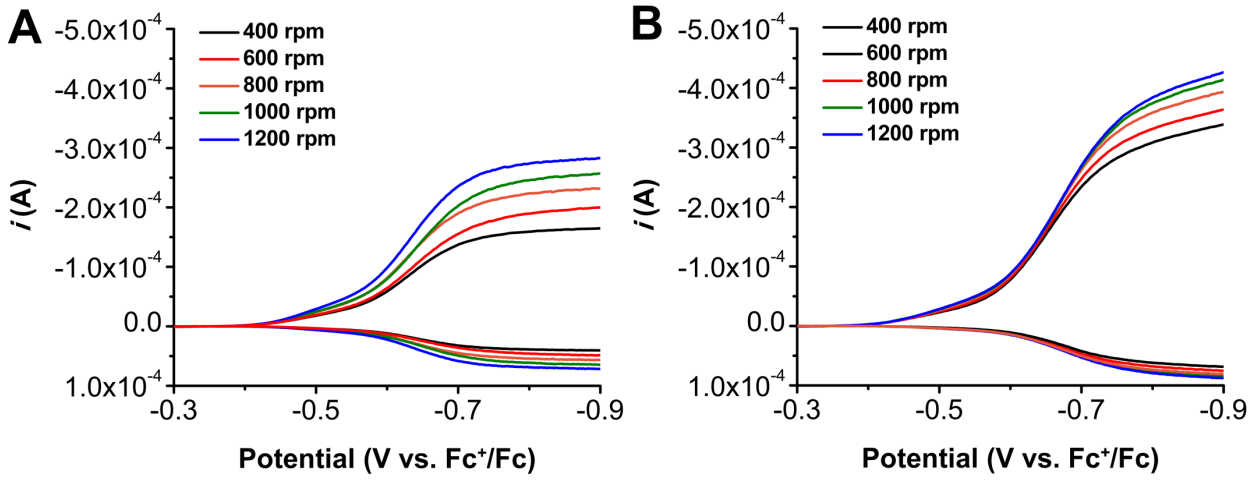

Figure S45. Linear Sweep Voltammograms of RRDE experiment with 0.5 mM Mn(^{tbu}dhbpy)Cl **1**, 0.5 mM BQ and 1.37 M TFEOH at various rotation rates under Ar (**A**) and O_2 (**B**) saturation conditions; ring potential = 0.85 V vs Fc^+/Fc. Conditions: glassy carbon working electrode/Pt ring working electrode, glassy carbon rod counter electrode, Ag/AgCl pseudoreference electrode; scan rate 0.02 V/s.

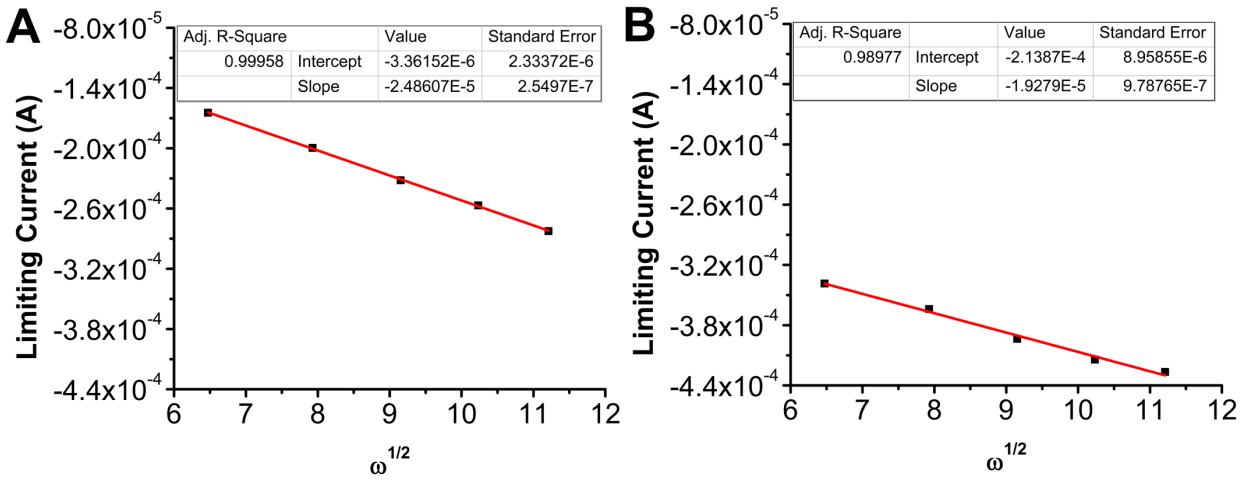

Figure S46. Levich plots from data obtained from Linear Sweep Voltammograms of 0.5 mM Mn(^{tbu}dhbpy)Cl **1** and 0.5 mM BQ by RRDE with 1.37 M TFE under Ar (**A**) and O_2 (**B**) saturation conditions at various rotation rates; ring potential = 0.85 V vs Fc^+/Fc.

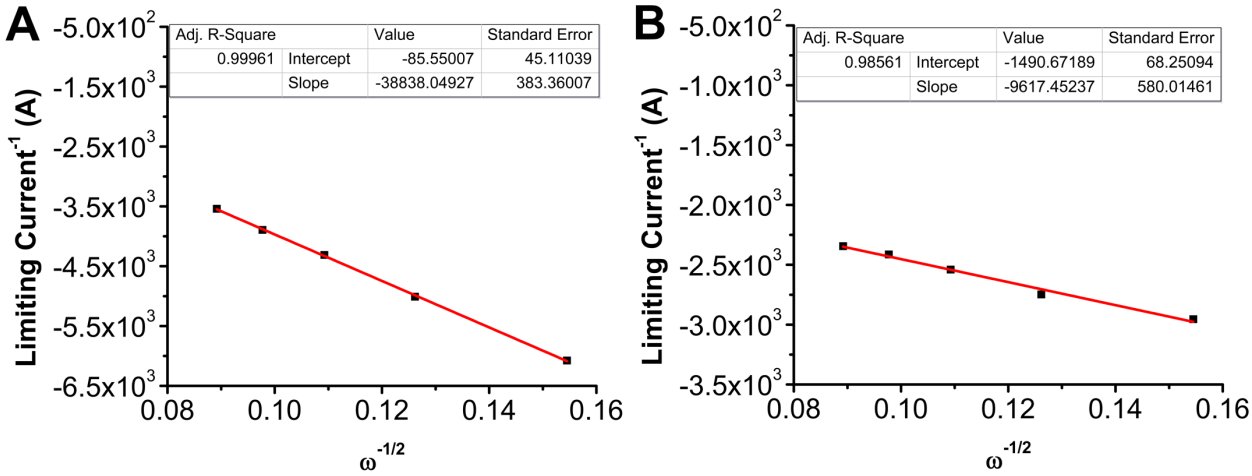

Figure S47. Koutecky-Levich plots from data obtained from Linear Sweep Voltammograms of 0.5 mM Mn(^{tbu}dhbpy)Cl **1** and 0.5 mM BQ by RRDE with 1.37 M TFE under Ar (**A**) and O_2 (**B**) saturation conditions at various rotation rates; ring potential = 0.85 V vs Fc^+/Fc.

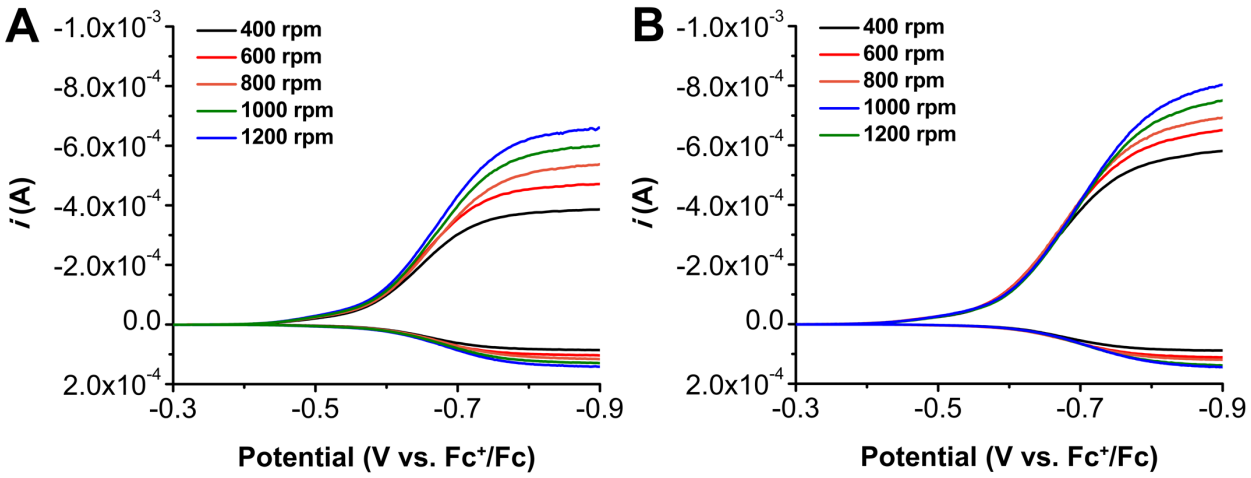

Figure S48. Linear Sweep Voltammograms of RRDE experiment with 0.5 mM Mn(^{tbu}dhbpy)Cl **1**, 1.25 mM BQ and 1.37 M TFEOH at various rotation rates under Ar (**A**) and O_2 (**B**) saturation conditions; ring potential = 0.4 V vs Fc^+/Fc. Conditions: glassy carbon working electrode/Pt ring working electrode, glassy carbon rod counter electrode, Ag/AgCl pseudoreference electrode; scan rate 0.02 V/s.

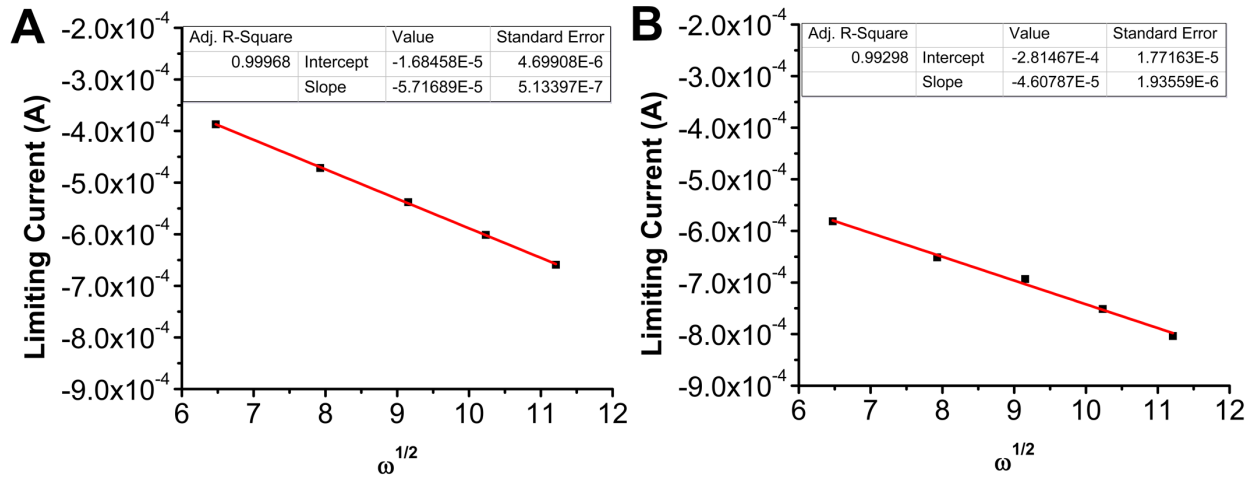

Figure S49. Levich plots from data obtained from Linear Sweep Voltammograms of 0.5 mM Mn(^{tbu}dhbpy)Cl **1** and 1.25 mM BQ by RRDE with 1.37 M TFE under Ar (**A**) and O_2 (**B**) saturation conditions at various rotation rates; ring potential = 0.4 V vs Fc^+/Fc.

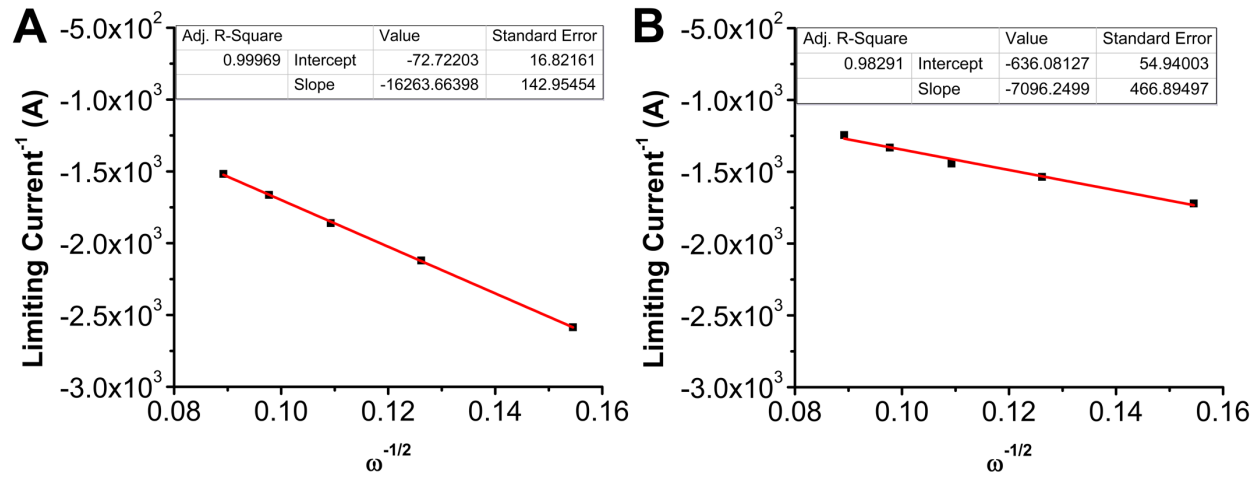

Figure S50. Koutecky-Levich plots from data obtained from Linear Sweep Voltammograms of 0.5 mM Mn(^{tbu}dhbpy)Cl **1** and 1.25 mM BQ by RRDE with 1.37 M TFE under Ar (**A**) and O_2 (**B**) saturation conditions at various rotation rates; ring potential = 0.4 V vs Fc^+/Fc.

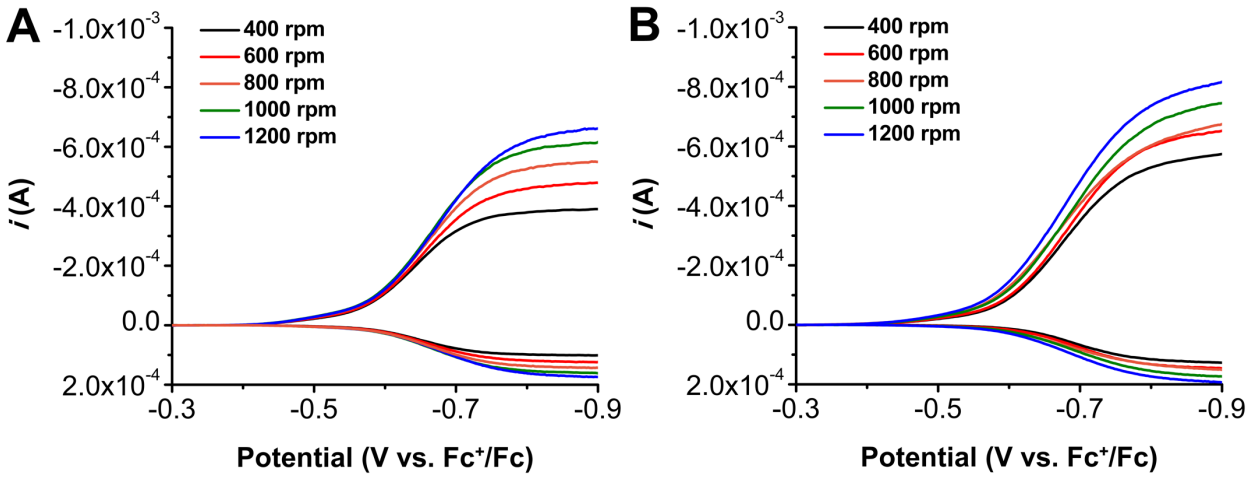

Figure S51. Linear Sweep Voltammograms of RRDE experiment with 0.5 mM Mn(^{tbu}dhbpy)Cl **1**, 1.25 mM BQ and 1.37 M TFEOH at various rotation rates under Ar (**A**) and O_2 (**B**) saturation conditions; ring potential = 0.85 V vs Fc^+/Fc. Conditions: glassy carbon working electrode/Pt ring working electrode, glassy carbon rod counter electrode, Ag/AgCl pseudoreference electrode; scan rate 0.02 V/s.

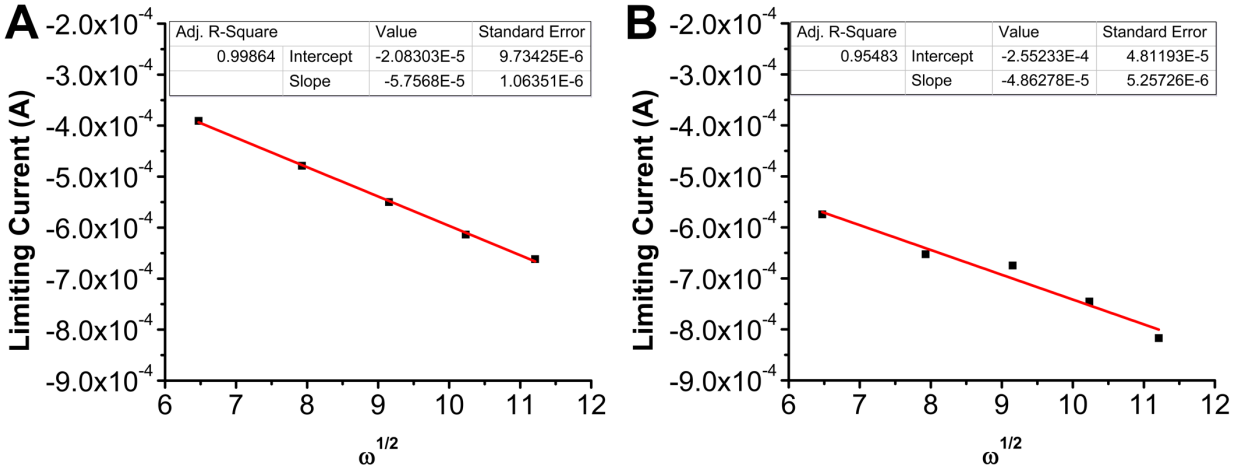

Figure S52. Levich plots from data obtained from Linear Sweep Voltammograms of 0.5 mM Mn(^{tbu}dhbpy)Cl **1** and 1.25 mM BQ by RRDE with 1.37 M TFE under Ar (**A**) and O_2 (**B**) saturation conditions at various rotation rates; ring potential = 0.85 V vs Fc^+/Fc.

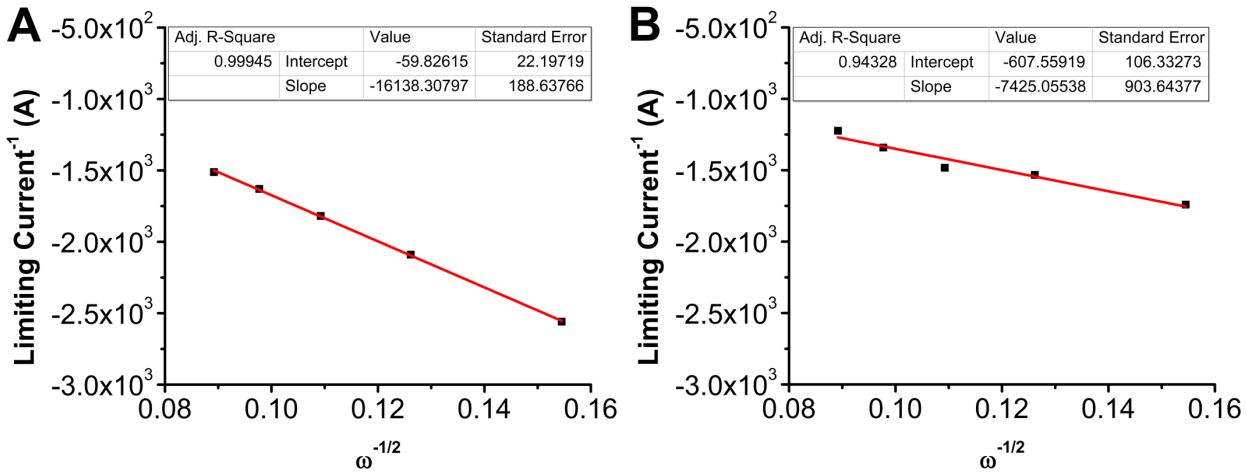

Figure S53. Koutecky-Levich plots from data obtained from Linear Sweep Voltammograms of 0.5 mM Mn(^{tbu}dhbpy)Cl **1** and 1.25 mM BQ by RRDE with 1.37 M TFE under Ar (**A**) and O_2 (**B**) saturation conditions at various rotation rates; ring potential = 0.85 V vs Fc^+/Fc.

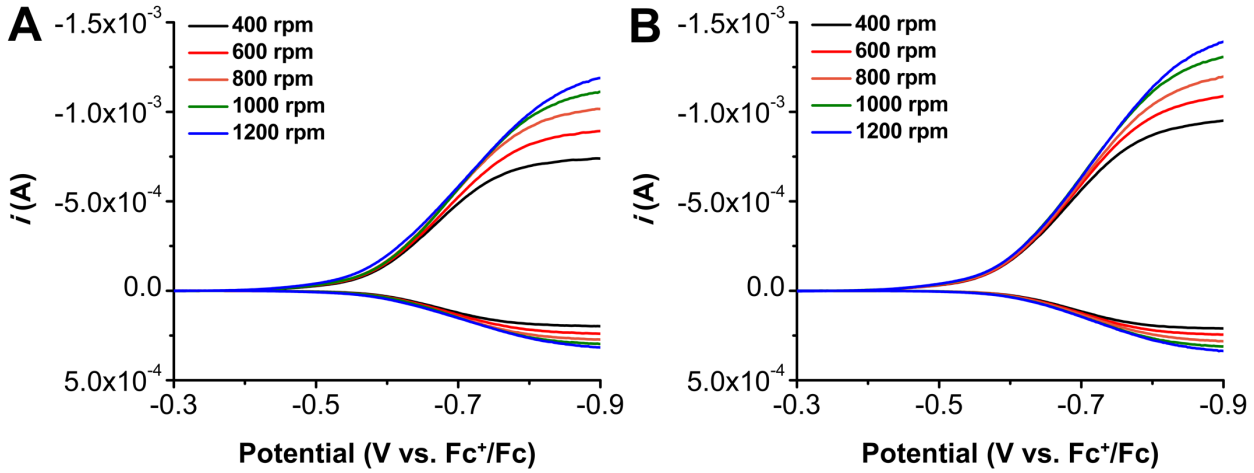

Figure S54. Linear Sweep Voltammograms of RRDE experiment with 0.5 mM Mn(^{tbu}dhbpy)Cl **1**, 2.5 mM BQ and 1.37 M TFEOH at various rotation rates under Ar (**A**) and O_2 (**B**) saturation conditions; ring potential = 0.85 V vs Fc^+/Fc. Conditions: glassy carbon working electrode/Pt ring working electrode, glassy carbon rod counter electrode, Ag/AgCl pseudoreference electrode; scan rate 0.02 V/s.

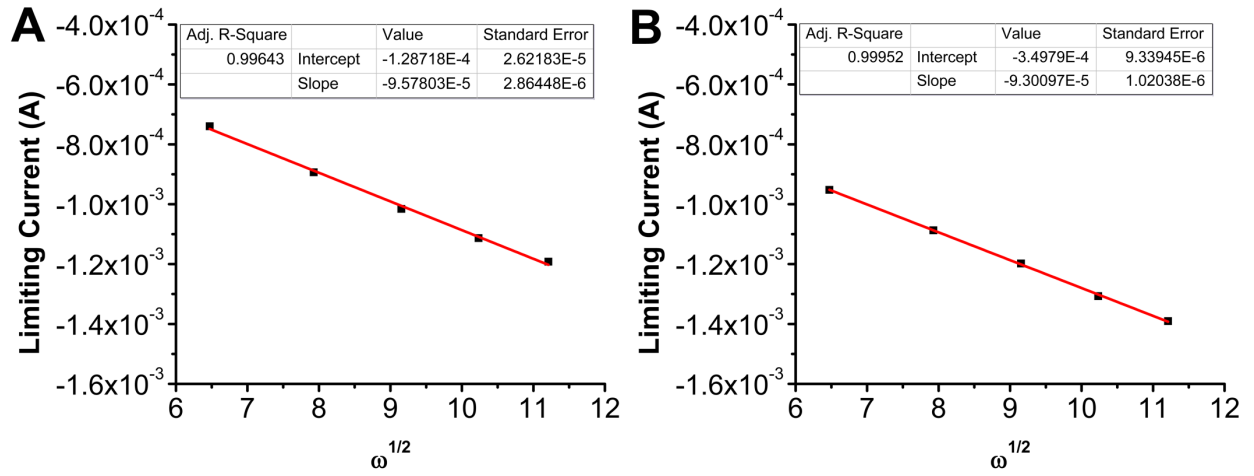

Figure S55. Levich plots from data obtained from Linear Sweep Voltammograms of 0.5 mM Mn(^{tbu}dhbpy)Cl **1** and 2.5 mM BQ by RRDE with 1.37 M TFE under Ar (**A**) and O_2 (**B**) saturation conditions at various rotation rates; ring potential = 0.85 V vs Fc^+/Fc.

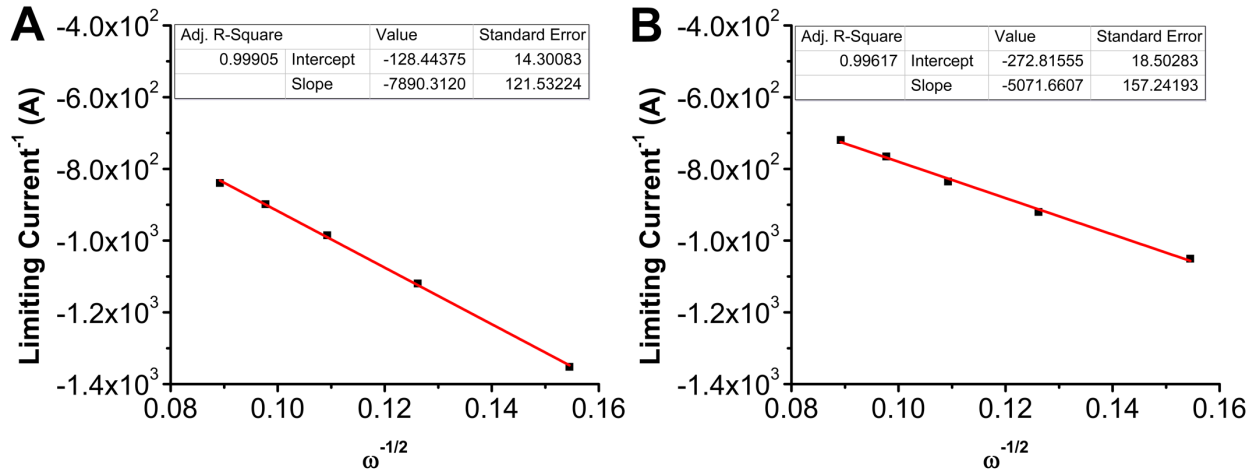

Figure S56. Koutecky-Levich plots from data obtained from Linear Sweep Voltammograms of 0.5 mM Mn(^{tbu}dhbpy)Cl **1** and 2.5 mM BQ by RRDE with 1.37 M TFE under Ar (**A**) and O_2 (**B**) saturation conditions at various rotation rates; ring potential = 0.85 V vs Fc^+/Fc.

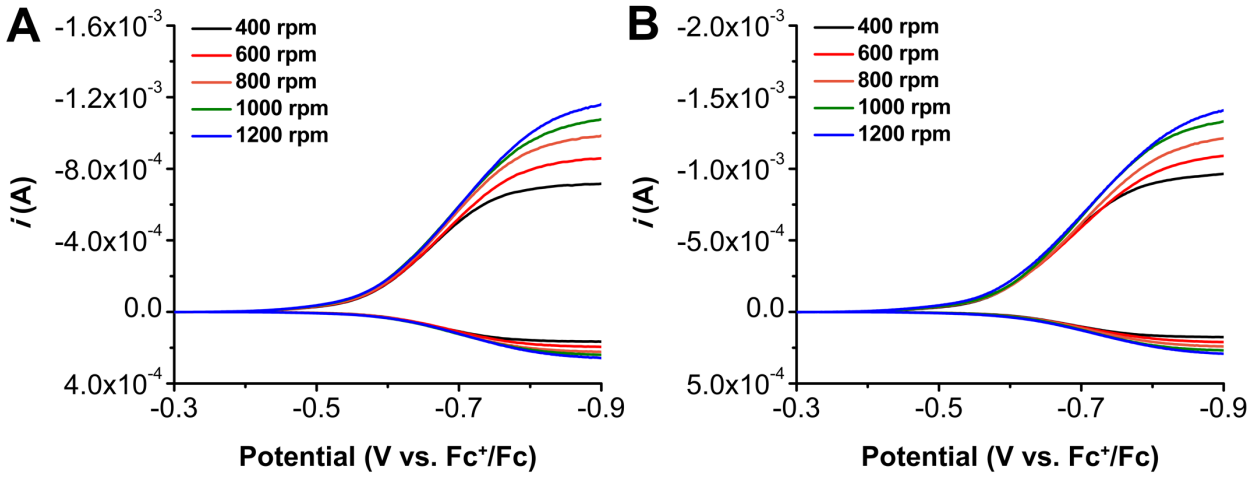

Figure S57. Linear Sweep Voltammograms of RRDE experiment with 0.5 mM Mn(^{tbu}dhbpy)Cl **1**, 2.5 mM BQ and 1.37 M TFEOH at various rotation rates under Ar (**A**) and O_2 (**B**) saturation conditions; ring potential = 0.4 V vs Fc^+/Fc. Conditions: glassy carbon working electrode/Pt ring working electrode, glassy carbon rod counter electrode, Ag/AgCl pseudoreference electrode; scan rate 0.02 V/s.

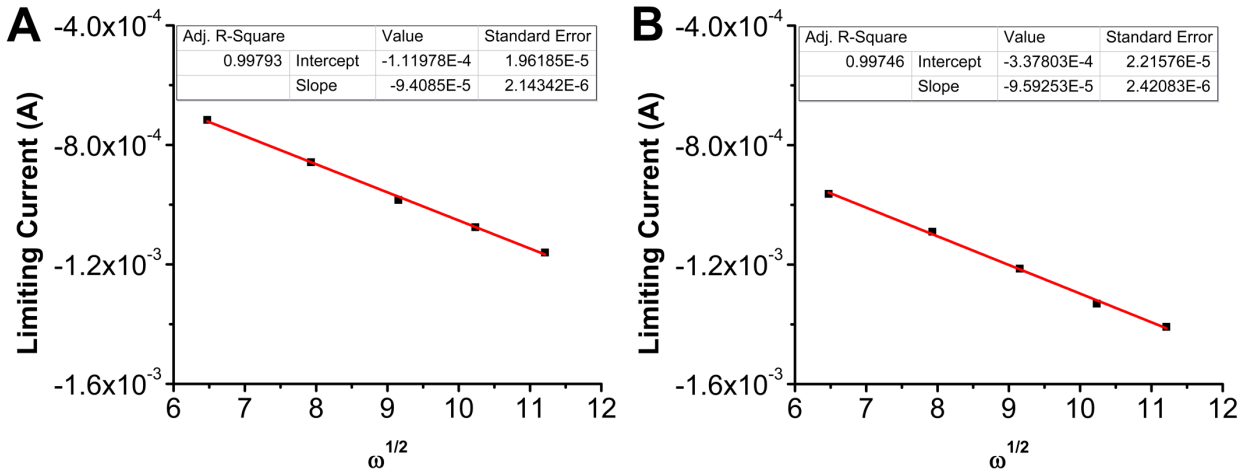

Figure S58. Levich plots from data obtained from Linear Sweep Voltammograms of 0.5 mM Mn(^{tbu}dhbpy)Cl **1** and 2.5 mM BQ by RRDE with 1.37 M TFE under Ar (**A**) and O_2 (**B**) saturation conditions at various rotation rates; ring potential = 0.4 V vs Fc^+/Fc.

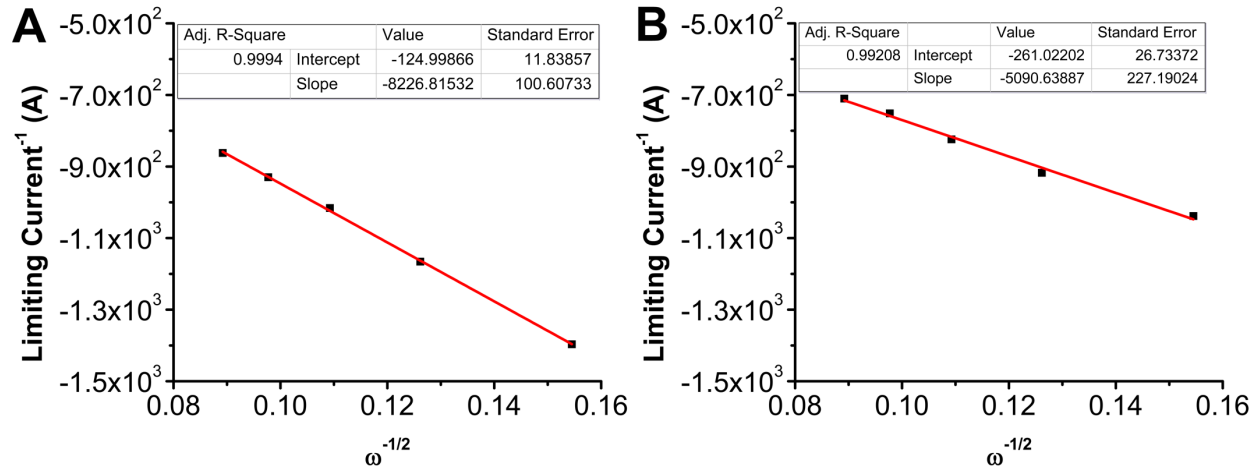

Figure S59. Koutecky-Levich plots from data obtained from Linear Sweep Voltammograms of 0.5 mM Mn(^{tbu}dhbpy)Cl **1** and 2.5 mM BQ by RRDE with 1.37 M TFE under Ar (**A**) and O_2 (**B**) saturation conditions at various rotation rates; ring potential = 0.4 V vs Fc^+/Fc.

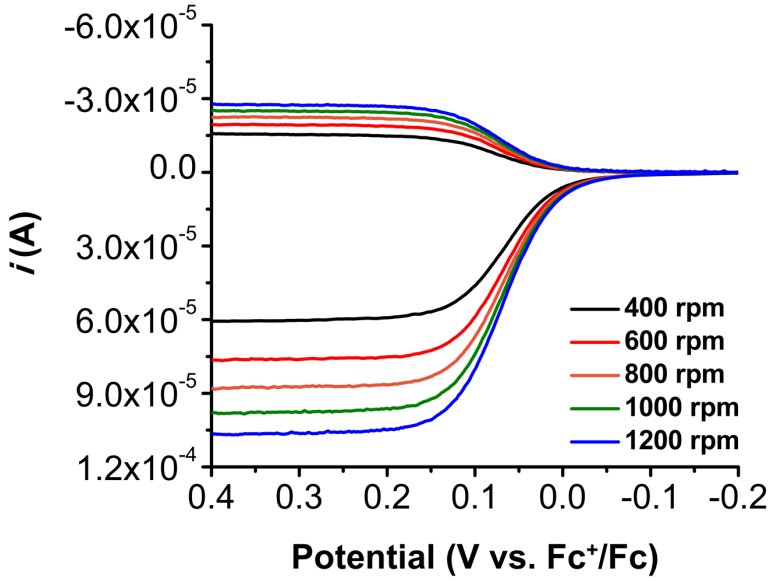

Figure S60. Linear Sweep Voltammograms of RRDE experiment with 0.5 mM ferrocene at various rotation rates under Ar saturation conditions; ring potential = 0.85 V vs Fc^+/Fc. Conditions: glassy carbon working electrode/Pt ring working electrode, glassy carbon rod counter electrode, Ag/AgCl pseudoreference electrode; scan rate 0.02 V/s.

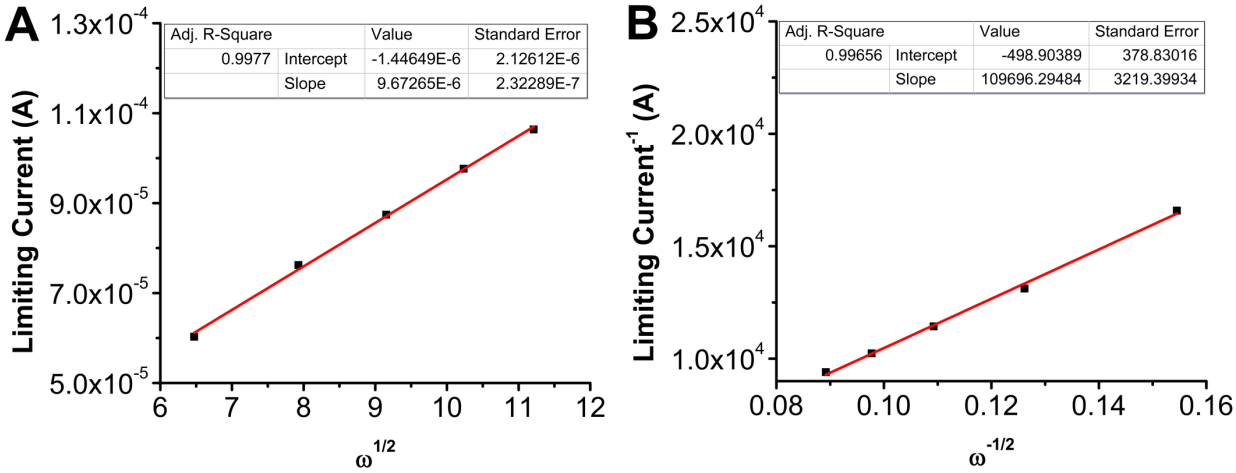

Figure S61. Levich (**A**) and Koutecky-Levich (**B**) plots from data obtained from Linear Sweep Voltammograms of 0.5 mM ferrocene by RRDE under Ar saturation conditions at various rotation rates; ring potential = 0.85 V vs Fc^+/Fc.

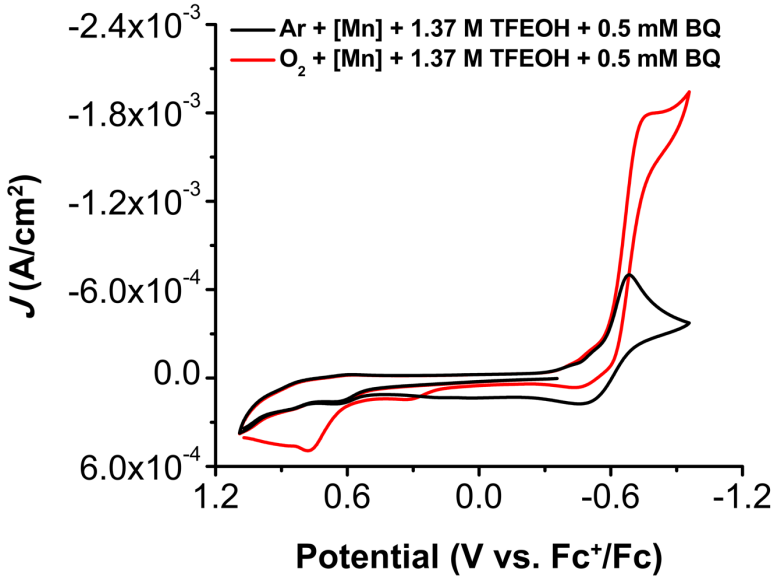

Figure S62. CVs of 0.5 mM Mn(^{tbu}dhbpy)Cl **1**, and 0.5 mM BQ obtained under Ar (black) and O_2 (red) saturation conditions with 1.37 M TFEOH. Conditions: 0.1 M $TBAPF_6$/MeCN; glassy carbon working electrode, glassy carbon counter electrode, Ag/AgCl pseudoreference electrode; 100 mV/s scan rate; referenced to internal ferrocene standard.

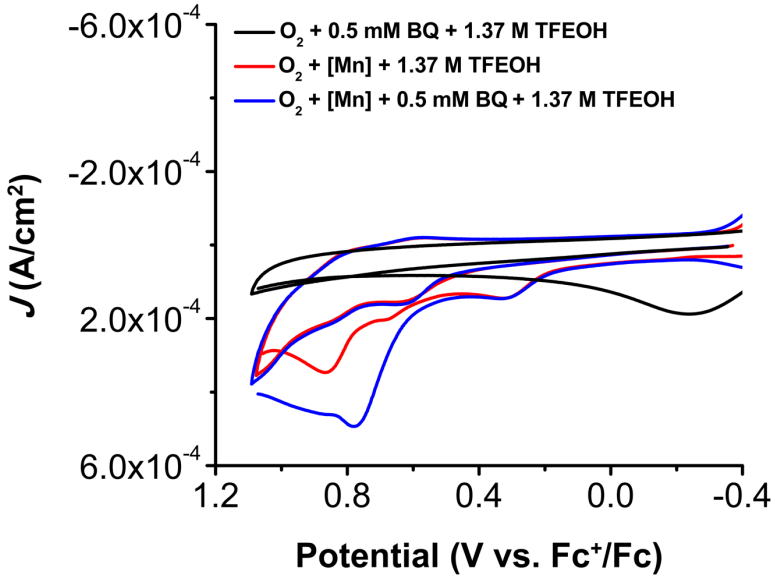

Figure S63. CVs of oxidative regions; all CV sweeps start at –0.35 V and proceed to an initial switching potential at +1.2 V, then to a second switching potential at –1.0 V, before sweeping to an ending potential of +1.2 V. Conditions: 0.1 M $TBAPF_6$/MeCN; glassy carbon working electrode, glassy carbon counter electrode, Ag/AgCl pseudoreference electrode; 100 mV/s scan rate; referenced to internal ferrocene standard.

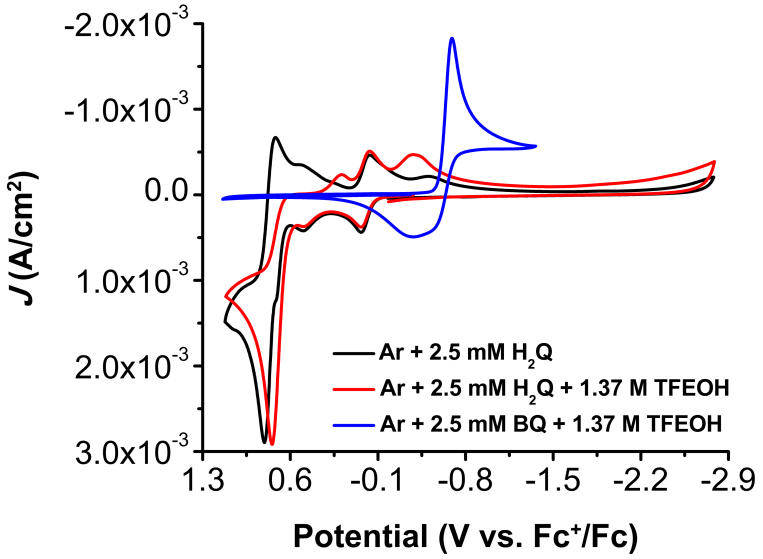

Figure S64. CVs of 2.5 mM H_2Q with (red) and without (black) TFEOH under Ar saturation conditions and comparable data under O_2 with BQ (blue). For all traces, the arrow indicates the initial sweep direction; the blue trace sweeps to positive potentials twice, before and after reducing potentials. Conditions: 0.1 M $TBAPF_6$/MeCN; glassy carbon working electrode, glassy carbon counter electrode, Ag/AgCl pseudoreference electrode; 100 mV/s scan rate; referenced to internal ferrocene standard. Arrow designates the direction of the CV trace.

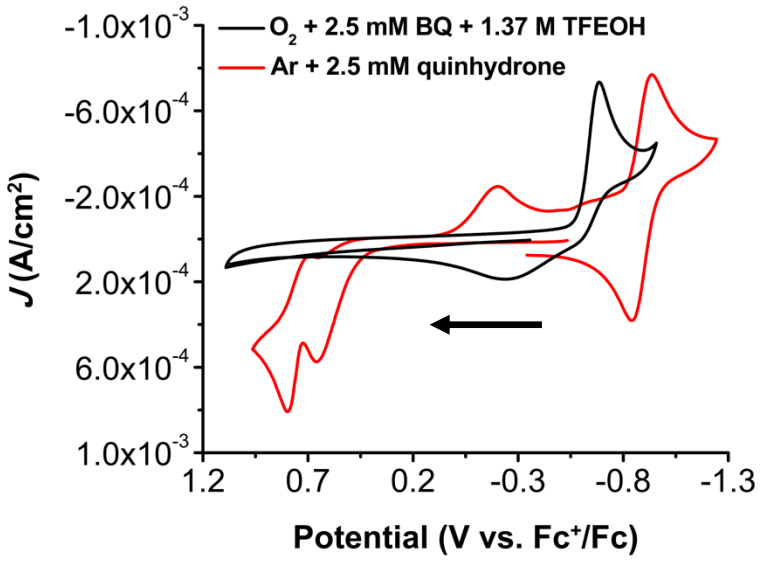

Figure S65. CVs with 2.5 mM quinhydrone under Ar saturation conditions (red) and 2.5 mM BQ with 1.37 M TFEOH under Ar saturation conditions (black). For all traces, the arrow indicates the initial sweep direction; the black trace sweeps to positive potentials twice, before and after reducing potentials. Conditions: 0.1 M $TBAPF_6$/MeCN; glassy carbon working electrode, glassy carbon counter electrode, Ag/AgCl pseudoreference electrode; 100 mV/s scan rate; referenced to internal ferrocene standard. Arrow designates the direction of the CV trace.

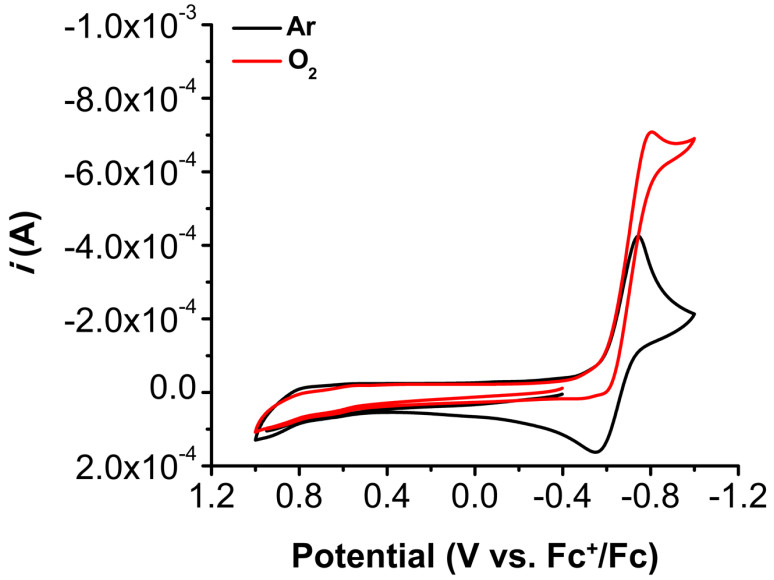

Figure S66. CVs obtained with the RRDE electrode used in this study with 0.5 mM Mn(^{tbu}dhbpy)Cl **1**, 2.5 mM BQ and 1.37 M TFEOH under Ar (black) and O_2 (red) saturation conditions. Conditions: 0.1 M $TBAPF_6$/MeCN; glassy carbon working electrode, glassy carbon counter electrode, Ag/AgCl pseudoreference electrode; 100 mV/s scan rate; referenced to ferrocene standard.

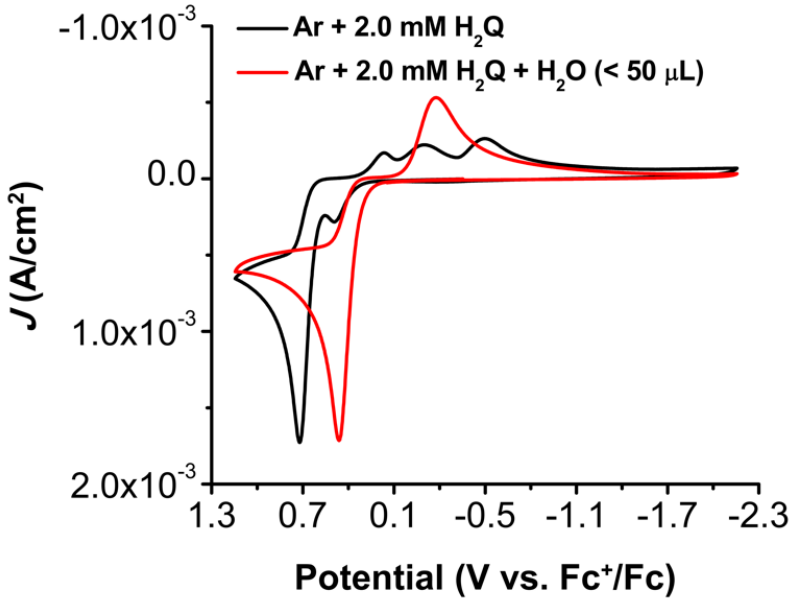

Figure S67. CVs of 2.5 mM H_2Q with (red) and without (black) added water under Ar saturation conditions. The data with added water closely match those reported for related studies by others,[2-3] who reported using solvent as received and did not recrystallize electrolyte. This indicates that the divergence we observe from these prior results in our own data is the result of residual water in the samples studied by others. Conditions: 0.1 M $TBAPF_6$/MeCN; glassy carbon working electrode, glassy carbon counter electrode, Ag/AgCl pseudoreference electrode; 100 mV/s scan rate; referenced to internal ferrocene standard.

References:

1. Gonzalez, F. J.; Astudillo, P. D.; Magali, S.; Macías-Ruvalcaba, N. A.; Bautista Martinez, J. A. A.; Aguilar-Martinez, M.; Gómez, M.; Frontana, C. E.; Gonzalez, I., Modifying the Reactivity of Reduced Intermediates of Quinones by Structural Changes and Intra and Inter Molecular Hydrogen Bonding. *ECS Transactions* **2019,** *3* (29), 25-36.
2. Astudillo, P. D.; Tiburcio, J.; González, F. J., The role of acids and bases on the electrochemical oxidation of hydroquinone: Hydrogen bonding interactions in acetonitrile. *Journal of Electroanalytical Chemistry* **2007,** *604* (1), 57-64.
3. Alligrant, T. M.; Alvarez, J. C., The Role of Intermolecular Hydrogen Bonding and Proton Transfer in Proton-Coupled Electron Transfer. *The Journal of Physical Chemistry C* **2011,** *115* (21), 10797-10805.